Lack of the myotendinous junction marker col22a1 results in posture and locomotion disabilities in zebrafish

Marilyne Malbouyres, Alexandre Guiraud, Christel Lefrançois, Mélanie Salamito, Pauline Nauroy, Laure Bernard, Frédéric Sohm, Bruno Allard, Florence Ruggiero

Lack of the myotendinous junction marker col22a1 results in posture and locomotion disabilities in zebrafish

Marilyne Malbouyres[1], Alexandre Guiraud[1*], Christel Lefrançois[2*], Mélanie Salamito[1], Pauline Nauroy[1], Laure Bernard[1], Frédéric Sohm[1], Bruno Allard[3] and Florence Ruggiero[1#].

[1] Université de Lyon, ENSL, CNRS, Institut de Génomique Fonctionnelle de Lyon (IGFL), Université Claude Bernard Lyon 1, Lyon, France.

[2] Littoral Environnement et Sociétés (LIENSs), UMR 7266CNRS- La Rochelle Université, La Rochelle Cedex 01, France

[3] Université de Lyon, Institut NeuroMyoGène (INMG), Université Claude Bernard Lyon 1, UMR CNRS 5310, Inserm U1217, Faculté de Médecine et de Pharmacie Rockefeller, Lyon, France

*Both authors equally contributed to this work

[#] Corresponding author

Florence Ruggiero

Institut de Génomique Fonctionnelle de Lyon - ENS de Lyon

46 Allée d'Italie

F69364 Lyon cedex 07, France

Phone number: +33 472722657

e-mail: florence.ruggiero@ens-lyon.fr

Key words: collagens, myotendinous junction, *col22a1*, locomotion, myopathy, zebrafish

Abbreviations: collagen XXII, ColXXII; DGC, dystrophin-glycoprotein complex; ECM, extracellular matrix; IMF, intermyofibrillar; MTJ, myotendinous junction; SSM, subsarcolemmal mitochondria; TEM, transmission electron microscopy; dpf, days post-fertilization; mpf, months post-fertilization; wpf, weeks post-fertilization

Abstract

The myotendinous junction (MTJ) is essential for the integrity of the musculoskeletal unit. Here, we show that gene ablation of the MTJ marker *col22a1* in zebrafish results in MTJ dysfunction but with variable degrees of expression and distinct phenotypic classes. While most individuals reach adulthood with no overt muscle phenotype (class 1), a subset of the progeny displays severe movement impairment and die before metamorphosis (class 2). Yet all mutants display muscle weakness due to ineffective muscle force transmission that is ultimately detrimental for class-specific locomotion-related functions. Movement impairment at the critical stage of swimming postural learning causes class 2 larval death by compromising food intake. In class 1 adults, intensive exercise is required to uncover a decline in muscle performance, accompanied by higher energy demand and mitochondrial adaptation. This study underscores *COL22A1* as a candidate gene for myopathies associated with dysfunctional force transmission and anticipates a phenotypically heterogeneous disease.

Introduction

The myotendinous junction (MTJ) is a specialized anatomical region where tendon collagen fibers insert into the muscle basement membrane. These muscle-tendon connection sites are appropriately located and organized to transmit muscle contractile forces to tendons and create a movement. This is mainly due to the presence of two independent trans-sarcolemmal linkage systems that structurally link the intracellular contractile elements of muscle cells to the extracellular matrix (ECM) of tendons, the dystrophin-glycoprotein complex (DGC) and the α7β1 integrin complex. Mutations in their associated genes, such as dystrophin, α-7integrin, and α-2 laminin have been associated with myopathies in patients and animal models revealing that most of the MTJ components are unconditionally required for proper muscle function and integrity [1,2,3]. The impact of these mutations in MTJ formation and/or function remains poorly documented, particularly in the context of human diseases for which biopsies at this particular location would be too prejudicial for the patients. Yet mice that lack dystrophin (*mdx; Dmd,* [4,5]), laminin α2 (*dy; Lama2,* [6]) or integrin α7 [7,8] all exhibit a striking reduction in the number of membrane folds at MTJ. Zebrafish has proven instrumental in the study of MTJ components in developing skeletal muscle. In zebrafish, mutant lines of the structural proteins enriched at the MTJ (*sapje/dystrophin*, *caf/lama2* and *patchytail/dag1)* or morpholino (MO)-knockdown in zebrafish embryos of *itga7, thbs4b,* or *col22a1* all displayed compromised muscle attachments that result in muscular dystrophies of various severities [9,10,11,12]. However *in vivo* function of these components was generally limited to zebrafish larval stage while muscular dystrophies are often progressive muscle disorders.

Collagen XXII (ColXXII) is a recognized marker of the MTJ that was first described by Koch and colleagues [13]. Functional analysis in zebrafish showed that *col22a1* expression concentrates at the ends of muscle fibers guiding the protein deposition at the junctional ECM. ECM proteome across muscle-tendon interface found ColXXII restricted to the muscle-tendon junction tissue [14]. Single-nucleus RNA-seq analysis in mice recently suggested that myonuclei near the muscle ends and tenocytes may both contribute this collagen [15]. While ColXXII binding partners have not been biochemically identified yet, synergistic interactions

suggested that ColXXII is a constitutive protein of the transmembrane α7β1 linkage system. In addition, transmission electron microscopy (TEM) revealed that ColXXII is located at the outer surface of the MTJ suggesting a structural role linking the basement membrane to the tendinous ECM [11,13]. As such, ColXXII could be the missing link that anchors muscle basement membrane network to the tendon collagen fibers. Although recognized as an important structural protein of the MTJ, the role of ColXXII in adult muscle function and performance remains overlooked. A recent study nonetheless described that high mRNA expression of *COL22A1* at the MTJ is associated with muscle injury risk in athletes [16].

Here, we generated loss-of-function mutants in zebrafish *col22a1* using CRISPR/Cas9 technology to detail the function of ColXXII beyond early larval stages. Phenotype discrepancy between morphants and knock-out (KO) stable lines have been previously reported [17,18,19]. But, as a rare example of a strong correlation between morpholino-induced and mutant phenotypes [17], we further documented the requirement of ColXXII for proper development of the myotendinous system, for contractile force transmission and ultimately movements not only in larvae but in adults. By combining ultrastructural analyses, muscle performance measurements and behavioral assays, we demonstrate that the lack of ColXXII results in the systematic dysfunction of the myotendinous unit that impairs postural behavior learning and swimming performance but with variable expressivity as often observed in human disease.

Results

Ablation of zebrafish col22a1 results in phenotypic variability

ColXXII morphant embryos showed dystrophic-like phenotype [11]. But muscular dystrophy demonstrates marked skeletal muscle phenotypic modulation [20]. Thus, to further analyze the function of *col22a1* in larvae and adults, we generated two distinct *col22a1* KO lines using CRISPR/Cas9 technology: *col22a1*^{vWA} *and col22a1*^{TSPN} lines that target exon 2 and exon 6, respectively (Figure 1A, Supplementary Figure 1). Whole-mount immunostaining with antibodies against zebrafish ColXXII [11] confirmed the complete extinction of ColXXII expression in homozygous *col22a1*$^{vWA-/-}$ and *col22a1*$^{TSPN-/-}$ mutants (Figure 1B).

At first, the *col22a1*$^{vWA-/-}$ and *col22a1*$^{TSPN-/-}$ fish appeared to develop normally and did not show any obvious muscular phenotype during embryo development. They hatched normally and successfully reached adulthood with no visible defects to the naked eye. If not genotyped, homozygous and heterozygous fish at 5 days post-fertilization (dpf) were phenotypically indistinguishable from their wild-type (WT) siblings. However, a closer examination of the survival rate of the mutant fish astonishingly revealed that about 30% of the fish between 5dpf and adult stage were lost in clear contrast with the average mortality observed in WT animals (2-3%) (Table 1). This percentage did not vary when *col22a1*$^{TSPN-/-}$ or *col22a1*$^{vWA-/-}$ individuals that have reached adulthood were incrossed (Table 1). A closer examination of larvae during their growth revealed that, while most mutant fish remained phenotypically normal and reach adulthood, a subset of the total population started to show discernable musculoskeletal abnormalities at approximately 2 weeks post-fertilization (wpf) (Figure 2A). Because this variability could be due to a difference in the RNA decay efficiency that might not have cleaned of all defective transcripts, we measured *col22a1* transcript levels on RNA extracts of trunks of the two phenotypic subpopulations of larvae with q-PCR. We showed that *col22a1* transcript levels dropped to almost zero in the two phenotypic subpopulations of the mutant lines (Figure 2C). The severe phenotypic traits discernable at about 2wpf larvae included impaired trunk movement and swimming capacities (Supplementary Movies 1-3) and a slight but significant reduction of the total body length (Figure 2A and B, quantification). These larvae prematurely died shortly afterward (Figure 2A and Table 1). The cause of their death, few hours after the critical 2wpf stage is not known. One likely explanation is the compromised food intake due to their impaired motility as we observed that the intestines of these larvae were optically empty compared to WT and homozygous mutants with no overt phenotype (Figure 2A).

In conclusion, lack of *col22a1* in zebrafish generates two distinct phenotypic classes in the progeny: “class 1”, showing no overt phenotype and “class 2” that prematurely dies at the critical premetamorphosis stage.

col22a1 mutants show variable deficits in the myotendinous unit structure and function

We next hypothesize that the striking difference in the severity of the phenotypes could be the result of incomplete penetrance or variable expressivity of a musculoskeletal phenotype. To address this question, we decided to measure electrically evoked muscle force generation of *col22a1*$^{TSPN-/-}$ mutant fish that grow to adulthood (class 1) and compare the values to *col22a1*$^{TSPN-/+}$ and WT siblings and the subset of *col22a1*$^{TSPN-/-}$ larvae that display severe musculoskeletal defects at 2wpf (class 2). Interestingly, the contractile force generated by *col22a1*$^{TSPN-/-}$ muscles from both phenotypic classes was considerably lower compared to WT siblings and the mean amplitude of the twitch response was about two to four times smaller than WT in *col22a1*$^{TSPN-/-}$ phenotypic classes, class 1 and class 2, respectively (Figure 3A). Tetanic forces were also significantly lower in class 1 *col22a1*$^{TSPN-/-}$ larvae with no overt musculoskeletal phenotype compared to WT and heterozygous fish, but again, class 2 larvae with early motility-defective phenotype showed even lower values (Figure 3B). Our findings thus unveiled that all *col22a1*$^{-/-}$ larvae developed a MTJ phenotype but the degree of the phenotype severity differed among *col22a1*$^{-/-}$ individuals. Therefore, we conclude that lack of ColXXII impacts the efficacy of muscle contraction and force in all *col22a1*$^{-/-}$ larvae but with variable expressivity.

We previously postulated that the observed reduced muscle performance of 5dpf *col22a1* morphants is the consequence of distended vertical myosepta and reduced MTJ folds that cannot transmit properly the muscle contractile force [11]. Thus, we next analyzed the ultrastructure of the junctional region between skeletal muscles from mutants showing severe or mild phenotype at 2wpf. Interestingly, 2wpf *col22a1*$^{TSPN-/-}$ trunk muscles revealed structural defects in the MTJ with a range of severity between class 1 and 2 phenotypes. The differentiation and overall organization of sarcomeres as observed with TEM appeared not affected by the lack of ColXXII in both phenotypic classes of *col22a1*$^{TSPN-/-}$ mutants (Figure 3C). In contrast, all 2wpf mutants showed reduced MTJ finger-like folds (Figure 3C and D, quantification) and an unusual high number of myoseptal fibroblasts, though not quantified (Figure 3C). Vertical myosepta were distended and contained loosely-organized collagen fibrils compared to controls but these defects are much more severe in class 2 than in class 1

mutants (Figure 3C). More specific to the class 2 mutants was the lack of muscle cohesiveness next to the MTJ (Figure 3C), but in striking contrast to *col22a1* morphants [11], only rare muscle fiber detachment at the MTJ site was observed with histology (not shown). Altogether, our data show here that lack of ColXXII at the MTJ results in muscle force weakness due to compromised contractile force transmission of contractile strength from muscle to myoseptal tendon.

We then analyzed the MTJ structure and morphology of *col22a1*$^{TSPN-/-}$ larvae and WT siblings at 5dpf, when it was impossible to distinguish larvae with mild and severe phenotype. For this analysis, *col22a1*$^{TSPN-/-}$ larvae were randomly selected before being processed. Also, before morphological analysis, larvae were subjected (stimulated) or not (unstimulated) to repeated electric stimulations in order to challenge MTJ resistance to contractile force as described in [11]. Bright field observations showed that abnormally wavy muscle fibers appeared in the *col22a1*$^{TSPN-/-}$ somites after electrostimulation but not in WT (Figure 4A). However, somite alteration did not change birefringence measurements of the trunk regardless of whether fish are electrostimulated or not (Figure 4B, quantification). Specifically, no massive muscle detachment that would otherwise result in a strong reduction in birefringence and the observation of degenerative dark patches in somites under polarized light (Figure 4B) or immunostained with antibodies to myosin light chain 1 (in red, Figure 4C) was observed even after repeated contractile activity in *col22a1*$^{TSPN-/-}$ mutants. This is suggestive of subtle phenotypical differences between MO-knockdown embryos [11] and CRISPR/Cas9 mediated KO lines. Finally, as observed at later stage in both phenotypical classes, an abnormally high number of fibroblasts were present in *col22a1*$^{TSPN-/-}$ myosepta as judged by the presence of nuclei that form a dotted line all along the vertical myosepta (in blue; Figure 4C).

We conclude that all mutants showed MTJ dystrophic phenotype with variable expressivity. In a subset of the progeny, these defects are more severe and have profound consequences on muscle fatigue due to inefficient muscle force transmission. Reduction in force transmission could be progressively detrimental for class-specific locomotion-related phenotype.

Expression of the myotendinous junction genes is differentially dysregulated in *col22a1* KO-associated phenotypic classes

To next address the question of possible gene compensation that can explain why *col22a1* KO results in variable expressivity of phenotype, we performed RT-qPCR on RNA trunk extracts of 2wpf class 1 and class 2 mutants and WT to analyze differential gene expression of selected genes. We chose genes of MTJ components, *e.g*. those of the linkage systems that are likely indirect or direct binding partners of ColXXII [11] (Figure 5A). We have previously shown a synergistic gene interaction between *col22a1* and *itga7* [11]. Variation in myoseptal ECM gene expression was also sought as damaged myoseptal ECM is a common trait of class 1 and class 2 larvae. These included *col1a1a* (collagen I), col12a1a and col12a1b (collagen XII), *tnmd* (tenomodulin) and *scxa* and *scxb (*the two scleraxis paralogs in zebrafish). First, the overall results showed that expression levels of the selected genes did not follow the same pattern in class 1 and class 2 larvae (Figure 5B). Second, knockout of *col22a1* led to expression activation of the myoseptal *col1a1a* as well as *fn1b* that is only expressed at the nascent MTJ solely in class 1 larvae. This is indicative of remodeling of the damaged MTJ and myosepta in class 1 larvae that might not occur in class 2 larvae as these genes were even downregulated compared to WT (Figure 5B). Expression of *lama2* and *dag1* both encoding proteins of the dystrophin-glycoprotein complex (DGC) was unchanged in larvae from both phenotypic classes, as well as the myoseptal *col12a1a* and its paralog *col12a1b*, and *col14a1* paralogs for whose protein products are structurally and functionally closely related to ColXII [21,22,23,24]. In contrast, expression of *itga7*, *lama4* and *thbs4b* and the tendon markers *scxa* and *scxb* and *tnmd* was downregulated in both mutant classes compared to WT (Figure 5B). Finally, *col21a1* that is closely related to *col22a1* [13] is one of the most upregulated gene among the analyzed genes in class 1 larvae but not in class 2. Our data suggest a common yet undescribed thread that connects the transcriptional regulation of these genes in *col22a1* mutants with mild (class 1) phenotype but not in severe (class 2) phenotype.

Class 2 larvae show erratic movements and postural defects

We next investigate the cause of the class 2 larva death before metamorphosis. Interestingly, observations of freely swimming larvae and movies strikingly revealed that a subpopulation of larvae from both *col22a1*$^{TSPN-/-}$ and *col22a1*$^{vWA-/-}$ larvae failed to maintain horizontal posture and displayed defects in buoyancy at a stage they should have acquired this behavioral capacity crucial for their survival [25,26] as in WT siblings (Supplementary Movies 1-3). Instead, class 2 larva stay in a vertical position because they are unable to compensate the downward drag of the head by initiating bouts, likely because of defective muscle contractile response (Supplementary Movie 3 compared to Supplementary Movie 1). In addition, when some affected individuals managed to swim, they never succeeded to reach out the microscope field of view, in striking contrast to 2wpf WT or mutant individuals with no overt motility phenotype (class 1) that reached out the observation field of view several times in the same time window (Supplementary Movies 1-3). Images extracted from videos detailed the erratic movements and the postural defects of the *col22a1*$^{TSPN-/-}$ and *col22a1*$^{vWA-/-}$ mutants compared to WT and class 1 mutant siblings (Figure 6A and B). In conclusion, movement problems that seriously affect “class 2” larvae prevent them to acquire horizontal swimming posture that may correlate with their inability to respond to swimming bouts at a critical time for larval survival. This confirms the cause of their death as the reduced swimming capacity of the larvae critically compromises food-intake, explaining the abnormal high frequency of empty-gut class 2 larvae shown in (Figure 2A).

Class 1 phenotype is characterized by muscle fatigue and mitochondrial adaptation to exercise

We next turn to the question of why class 1 mutants do not display musculoskeletal system dysfunction. Because these mutants can reach adulthood, we have been able to measure muscle performance using a swimming tunnel respirometer that is intended to cause fish to fatigue. Fish are placed in a tunnel where water flow is increased stepwise and the capacity of the fish to swim against the current is scored (Figure 7A). U_{crit} represents the critical swimming speed originally defined as the maximal velocity a fish can reach during a swimming step

protocol [27]. In the meantime, measurements of the fish oxygen consumption during swimming tests allowed to determine the associated costs in oxygen. Two identical 170mL swimming respirometers were used in parallel and the protocol used was as depicted in Figure 7A. The tested 6mpf WT females and males showed similar U_{crit} values, therefore the mutant fish were selected for U_{crit} measurements regardless of their gender. As shown in Figure 7B, WT have no difficulty to swim against the flow at 5 Body Length.s^{-1} [BL.s^{-1}]) (Figure 7B, fish 1; Supplementary Movie 4), and even at higher speed (6.5 to 8 BL.s^{-1}) (Figure 7B fish 2-3; Supplementary Movies 6). On the contrary, *col22a1*$^{TSPN-/-}$ fish swam in a steady way at a moderate speed (5BL.s^{-1}) (Figure 7B fish 4 and 7; Supplementary Movie 5) but were unable to sustain the effort to counter-current swimming at higher speed (6.5 to 8 BL.s-1) and their caudal fin touched several times the honeycomb in the swimming chamber (Figure 7B fish 5-6 and 8-9; Supplementary Movie 7). Measurements of U_{crit} confirmed our observations as U_{crit} mean of class 1 mutant fish was statistically lower (6.98 ± 2.08 BL.s^{-1}) than in WT (10.89 ± 1.05 BL.s^{-1}) (Figure 7C, left panel). Similar results were obtained with *col22a1*$^{vWA-/-}$ fish (Figure 7C, right panel).

During exercise, requirements for oxygen in skeletal muscle is increased. Oxygen consumption was measured during swimming tunnel experiments and showed that mutant fish consume significantly more oxygen than WT over the course of the experiments (p_value= 0.00005) (Figure 8A). This could be explained by an increased trunk muscle activity in mutant fish to compensate for muscle weakness (Figure 3). Skeletal muscle mitochondria are essential to provide the energy required for movement. Resistance exercise drives skeletal muscle mitochondrial adaptations [28]. We thus postulated that, because of the class 1 *col22a1-/-* fish muscle weakness, the continuous effort required to freely swim in the tank or even more to swim against the current results in a significant increased oxygen consumption that might impact mitochondrial biogenesis.

To address this question, we next examined with TEM the ultrastructure of mutant and WT trunk muscle subjected to the swimming tunnel assay (challenged fish; Figure 8B). As observed in 2wpf mutant larvae, the most striking ultrastructural trait was the complete lack of

MTJ finger-like structures in mutants compared to WT while the skeletal muscle fibers appeared normal (Figure 8B). The observation of mitochondria revealed additional differences. There are two distinct mitochondria subpopulations in skeletal muscle: the subsarcolemmal mitochondria (SSM) and the intermyofibrillar mitochondria (IMF) that are found between myofibrils. They can be distinguished on the basis of their morphological features, IMF mitochondria being more elongated and thinner than SSM ones [29]. This different morphology was easily identified with TEM (Figure 8B). Interestingly, IMF mitochondria, but not SSM, seemed more numerous in mutant fish compared to WT (Figure 8B). This was confirmed by quantification of IMF and SSM subpopulations in mutant and WT trunk muscle (Figure 8C). We conclude that class 1 adult fish have to compensate their muscle weakness due to defective contractile force transmission by increasing muscle contractile activity and metabolism probably through mitochondrial adaptation.

Discussion

Although the MTJ is a common location for strain injuries in sports [30], little work has focused on the interface between muscle and tendon. Therefore, how defects in MTJ integrity impacts muscle contractile force transmission have been largely overlooked. We previously shown that ColXXII MO-knockdown in developing zebrafish embryos results in the appearance of a dystrophic-like phenotype in morphants [11]. The recent development of gene editing in zebrafish has brought the use of morpholinos into question [31,18]. Discordance between the MO-knockdown and knockout phenotypes has been attributed to different reasons including off-target effects of morpholinos. The traits we observed in the two *col22a1* mutants we have generated here are reminiscent to those observed in 5dpf *col22a1* morphants [11]. Nevertheless, our data unveil additional reasons for phenotypic discrepancies as possible inappropriate phenotypic analyses that prevent subtle phenotype from being revealed in genetic mutants. Also, experimenters might have not noticed the early death of developing embryos and larvae due to the large number of offspring and therefore have only analyzed the fish that display non overt phenotype.

We found that lack of *col22a1* results in two apparent extreme phenotypic classes found in both KO zebrafish lines: *col22a1*$^{-/-}$ larva that fail to propel in swim bouts and eventually cause the *col22a1*$^{-/-}$ larva to die by starvation at around 2wpf (class 2), and *col22a1*$^{-/-}$ larva that survive to adulthood without apparent abnormalities (class 1). Nevertheless, ultrastructural analysis of the *col22a1*$^{-/-}$ mutants reveals that the two distinct phenotypical classes share common myotendinous structural defects at the junctional ECM, though with variable grade of severity: (i) the distention of myosepta that atypically contain loosely-arranged and sparse collagen fibrils and (ii) a marked reduction of MTJ sarcolemmal folds that function is to optimize force transmission at the MTJ by increasing resistance to tensile strength. Rather, morphology of the trunk muscle and the ultrastructure of muscle fiber contractile apparatus appeared normal in both phenotypic classes. Combined ultrastructural and physiological studies revealed that ColXXII deficiency is functionally associated with an unusual MTJ phenotype. Hence, the ColXXII deficiency ultrastructural phenotype is rarely observed among others MTJ mutants or morphants. To our best knowledge, a substantial reduction of MTJ sarcolemmal folds was only reported in *itga7* KO mice displaying progressive muscular dystrophy [7,8] while abnormal vertical myosepta ultrastructure with abnormal blisters within the ECM was described in the zebrafish dystrophic mutant *softy* caused by a missense mutation in *lamb2* gene [32]. Pertaining to this observation, synergistic gene analysis in ColXXII morphants has suggested that ColXXII is part of the integrin $\alpha7\beta1$ linkage system [11]. Here we add evidence to this assumption by showing that in absence of *col22a1*, *igta7* expression but not *dag1* or *lama2* is down-regulated in class 1 and 2 larvae.

The degree of severity of the ultrastructural defects of the mutants MTJ correlates with their contractile transmission capacity as evidenced by electrically-evoked muscle contractile performance measurements and results in distinct locomotor-related behavior. The class 2 mutants displayed striking postural defects, a yet undescribed phenotype in other MTJ mutants. The capacity to correct the vertical posture is acquired at around 15-20 dpf when they begin to swim [25]. At that stage, larvae are able to re-adjust their posture by swimming bouts, a way to fight against gravity, and to this end, larvae control the speed and length of muscle

contractions. Zebrafish, as all teleosts, have a denser head than tail and thereby they have to correct the destabilizing nose-down rotations to swim [26]. Maintenance of posture requires continuous active sensorimotor control. Our findings revealed timely unexpected functional consequences of the MTJ ultrastructural defects. In *col22a1*$^{-/-}$ larvae, postural behavior is defective secondary to ineffective muscle force transmission. As such, muscle contractile activity is reduced, swimming bouts are ineffective and the vertical posture cannot be fought. This in turn injured the chances of *col22a1*$^{-/-}$ larvae to swim and search for food resulting in starving to death, this latter assumption being supported by the empty-gut phenotype of class 2 larvae.

Contrary to class 2 mutants, the structural defects in the myotendinous unit did not seem to affect dramatically class 1 larval motility, swimming capacity or posture although electrically-evoked contractile force measurements of the trunk musculature revealed muscle weakness. Class 1 adult fish had to be subjected to swimming-induced exercise to reveal the functional consequences of *col22a1* gene ablation in zebrafish. We showed that these fish rapidly developed muscle fatigue and reduced swimming capacity due to defective force transmission capacity resulting from MTJ ultrastructural defects. O_2 consumption was substantially increased in class 1 mutants during swimming performance assays. One plausible explanation is that during sustained swimming activity, *col22a1*$^{-/-}$ zebrafish have to initiate skeletal muscle contractions more often for a same effort to compensate for muscle weakness. This likely entailed a higher energy demand. This is consistent with the increase in oxygen demand observed during the swimming challenge as class 1 mutant adults consumed more oxygen than WT for a same effort. Along this line, a higher number of IMF mitochondria was observed in class 1 muscle fibers. Acute increased in contractile activity patterns, as during exercise training (endurance or intermittent), was reported to favor mitochondria biogenesis [33]. The daily swimming activity of class 1 fish might require an increased energy demand as the force transmission capacity is defective in these mutants, that can provoke a mitochondrial adaptation over the long term. In addition, IMF mitochondria have been associated to energy production for contractile activity [34]. In that, our data suggested a mastryoshka doll-like

mechanism by which defective MTJ activity resulted in useless force transmission that could subsequently increase muscle contraction frequency, which in turn augment the overall muscle energy demand that led to training-induced mitochondrial adaptation.

Finally, our finding raised the question of why lack of *col22a1* gene produces different phenotypic patterns. The relationship between genotype and phenotype is not simple particularly in ECM genes [35,36,37]. This can be due to incomplete penetrance or variable expressivity, two events often observed in human inherited connective tissue disorders [38]. This was also reported as a possible mechanism to explain the reported phenotypic discrepancies in zebrafish, specifically when mutant phenotype was compared to the morphant one [19,39]. As discussed above, in our study the phenotype of our CRISPR/Cas9 *col22a1* mutant lines mostly recapitulates the one reported for *col22a1* morphants that also display gradient of phenotypic severity [11], these phenomena may account for the surprising apparent lack of phenotype in class 2 mutants. But gene compensation can also be invoked to explain this discrepancy [40]. In support to this assumption, differential dysregulation of MTJ gene expression occurred in class 1 but not class 2 mutants. A significant activation of *col21a1*, a *col22a1* closely-related gene and *col1a1a* are observed in class 1 but not class 2 larvae. *col21a1* gene has the particularity to be present in zebrafish and human genomes, but not in rodent genomes [41]. The function of this gene is still unknown. *col21a1* transcript is expressed in developing fish but its expression pattern is still unclear (Malbouyres M and Ruggiero F, personal communication, 03/2020). Instead, the upregulation of *col1a1a* in class 1 mutants can be interpreted as a way to compensate the reduced density of collagen fibrils in mutant myosepta and maintain to some extent the MJT activity. In support to this assumption, a high number of fibroblasts, the main cell source of collagen I, was abnormally observed in *col22a1* mutants, though independently on the phenotypic classes. Scleraxis is a transcription factor highly expressed in tendons that has been shown to regulate expression of collagen I genes in developing tendons in mice [42]. Expression of the two zebrafish paralogs, *scxa* and *scxb*, was found downregulated in both class 1 and 2 larvae, we can thus exclude that upregulation of *col1a1* in class 1 larvae results from an increase of scleraxis activity. Nevertheless, several

points remain obscure. Specifically, we cannot explain the severity of the *col22a1* phenotype in 30% of the larvae while about 70% display a mild phenotype. This will require further investigation including the search for expression of gene modifiers as recently reviewed [43]. In conclusion, the myotendinous disorder described here is unusual in that it is not associated with defects in muscle fiber ultrastructure and/or alteration of the contractile unit function but with useless force transmission that results in posture and locomotion disabilities. In that respect, *COL22A1* should be viewed as a candidate gene for human muscular dystrophies with unresolved genetic cause. Our study also provides a valuable genetic tool to investigate variable expressivity often observed in connective tissue human diseases and that represents an important point to consider for the design of chemical screens.

Materials and Methods

Zebrafish strain, maintenance, specific treatments and ethics statement

Zebrafish (AB/TU) were raised and bred according to standard procedures [21] (PRECI, SFR Biosciences UAR3444/CNRS, US8/Inserm, ENS de Lyon, UCBL; agreement number C693870602). The developmental stages are given in hours (hpf), days (dpf), weeks (wpf) and months (mpf) post-fertilization at 28°C, according to morphological criteria. For optimal growth during the first ten days, the embryos (30 individuals per 300 ml) are kept in tanks filled with water at least 5 cm deep and raised at 28.5°C. Then, the water volume is progressively increased to 900mL and the water circuit is open. At 6dpf, embryos are fed three times a day (Gemma75). From 12dpf, embryos are fed with live brine shrimp every day. Tricaine (ms-222, Sigma-Aldrich, St Louis, Missouri, USA) was used to anesthetize fish. From 24hpf, embryos were treated with phenylthiourea (P7629, Sigma-Aldrich, St Louis, Missouri, USA) to prevent pigmentation. All animal manipulations were performed in agreement with EU Directive 2010/63/EU. The creation, maintenance and use of *col22a1*$^{TSPN-/-}$ and *col22a1*$^{vWA-/-}$ lines were approved by the local ethics committee (CECCAPP_IGFL_2014_002 and CECCAPP_PRECI_2017_003) and all procedures have been approved by the French ethical committee (APAFIS#13345-2017113012206024v3).

Generation of CRISPR/Cas9 KO lines

DR274 gRNA plasmids and Cas9 protein were from Addgene (Cambridge Massachussets, USA) and New England Biolabs (Ipswich, MA, USA), respectively. CRISPR gRNAs were designed using CRISPR design software (http://crispor.tefor.net/ and http://crispr.dbcls.jp/). Different sgRNAs have been tested and we selected the two with the highest mutagenesis efficiencies. The DNA binding sites targeted by these sgRNAs are localized in the vWA domain (5'-GGATAAGACACGTGTGGCAG -3') and in the TSPN domain (5'-GGATGGCGAGAACAGGGCGG -3'). Oligonucleotides were annealed in a thermo block at 95°C for 5 min followed by a slow cooling to room temperature (≈25°C) and cloned in DR274 gRNA plasmid between BsaI sites. All constructs were verified by sequencing. To make gRNA, the template DNA was linearized by DraI (NEB-R0129) digestion and purified using a NucleoSpin Gel and PCR Clean-up (#740609, Macherey-Nagel, Duren, Germany) kit. gRNA was generated by *in vitro* transcription using a T7 MEGAscript transcription kit (AM1334-Thermo Fisher Scientific, Waltham, Massachussets, USA). After *in vitro* transcription, the gRNA was purified using ammonium acetate precipitation and stored at -80°C. Cas9 protein (2.12 ng) (New England BioLabs Inc. Ipswich, MA, USA,) and gRNA (133 pg) were co-injected in the cell at the one-cell stage and a quarter of the lay was used to evaluate mutagenesis efficiency by HRMA as previously described [44].

Genotyping

For gDNA extraction, embryos or fin clip were placed in PCR tubes in 200µL of NaOH 50mM, incubated 10 minutes at 95°C and immediately placed on ice. 20µL of Tris-HCL 1M pH8 were added to buffer the solution and gDNA were stored at 4°C. The primers used to genotype *col22a1*^{vWA} *and col22a1*^{TSPN} mutants were designed using Primer 3 Plus software (www.bioinformatics.nl/cgi-bin/primer3plus/primer3plus.cgi), genotyping : F-5'CCAGGTTGTAAGAACGTCCAC3'/R-5'GAACAACCTGATCCCAGCAG3' (for *col22a1*^{vWA}) and F-5'CATCCCGTAAGGAAGACTGG3'/ R-5'GATGGGTAGCGTCTCGATGT3' (for

col22a1^{TSPN}*)*. The amplicons for each line were run simultaneously in a 2% agarose gel and were sequenced.

RNA extraction and quantitative real-time PCR

Total RNA was isolated using Trizol (Invitrogen, Waltham, Massachussets, USA). Reverse transcription was performed using M-MLV reverse transcriptase (Promega, Fitchburg, Wisconsin, USA) for 1h at 37°C in presence of random hexamers (Promega). qPCR primers (Supplementary Table 1) were designed to produce amplicons of approximately 200 bp. qPCR was performed using a SYBR Green mix and fast amplicon protocol according to manufacturer instructions (Roche, Penzberg, Germany). Data were analyzed using the Ct method and normalized to *polr2d.* Data were analyzed using one-way ANOVA and tukey's post hoc tests (n=3).

Immunofluorescence staining

Whole-mount staining was performed as described previously [21]. Whole-mount embryos were observed with a Zeiss LSM 780 spectral confocal microscope (Zeiss, Oberkochen, Germany). The primary and secondary antibodies used in this study are listed in (Supplementary Table 2). Nuclei were stained with Hoechst solution and F-actin with fluorescent phalloidin conjugates (all from Sigma-Aldrich, St Louis, Missouri, USA)

Birefringence assay

WT or *col22a1*$^{TSPN-/-}$ 5dpf larvae were anesthetized with tricain, placed on a glass slide between two polarizers (3Dlens, Taiwan) and observed with a Zeiss Axiozoom V16 equipped with a AxioCam MRm 1.4 megapixels camera before and after electrostimulation. For quantification of birefringence, mean gray values of the trunk region of the different groups of larvae (n=10) were measured using ImageJ software (n=10). Data were analyzed using one-way ANOVA.

Transmission electron microscopy (TEM)

Zebrafish embryos and larvae were fixed in 1.5% (v/v) glutaraldehyde and 1.5% (v/v) paraformaldehyde in 0.1 M cacodylate buffer (pH 7.4) several days at 4°C followed by washing in 0.1 M cacodylate buffer, 8% sucrose (10 minutes, 3 times). Then, samples were quickly washed in distilled water. After post-fixation in 1% osmium tetroxide in 0.1 M cacodylate buffer, 8% sucrose for 45 minutes at room temperature, samples were dehydrated in graded series of ethanol (30 to 100 %), 5 minutes each, and propylene oxide during 10 minutes. Finally, samples were embedded in epoxy resin. Ultrathin sections were stained with 7% uranyl acetate in methanol and lead citrate, and observed with a Philips CM120 electron microscope equipped with a Gatan Orius 200 2Kx2K camera or a Jeol 1400 Flash equipped with a camera Gatan Rio16 (Centre Technologique des Microstructures, Université Lyon 1, France).

For adult muscle tissues, 6-months trunk muscles were dissected in the fixative buffer under stereoscopic control and skin was delicately removed thanks to tweezers. Those thicker samples were treated as described above but with an extended sample incubation time (15 mins for each step). An additional 15 mins incubation in propylen oxide/ethanol 100% (v/v) followed by incubation in propylen oxide were performed. Times of incubation during the embedding steps were also prolonged.

Quantification of mitochondria subpopulations and sarcolemma length at the MTJ were performed on TEM images at same magnification using ImageJ software.

Muscle force measurements

Procedures and measurements were performed as previously reported [11]. Larvae are briefly placed in a beaker containing 0.168 mg/mL of tricain (3-amino benzoic acidethylester, Sigma-Aldrich, A5040). The head is then crushed and larvae are transferred to a Tyrode physiological solution containing (in mM) 140 mm NaCl, 5 mm KCl, 2.5 mm $CaCl_2$, 1 mm $MgCl_2$, 10 mm Hepes, pH 7.2. Under binocular control, fish head and tail extremities were glued with surgical glue (Histoacryl, B Braun) on homemade thin aluminium foils pierced with a small hole allowing to attach the head portion of the fish to the arm of an AE801 force transducer and the tail portion to a fixed pin. Fish were stimulated by field electrodes placed on either side of the fish

using a Harvard apparatus 6002 stimulator. In each fish, the voltage of 0.5 ms duration pulses was increased to give maximal twitch response and the voltage used for measuring maximal force was set at 20 % above this maximal value. The fish was then gradually stretched on the side of the transducer moved with a micromanipulator until maximal twitch force was obtained. The force signal was recorded at 10 kHz sampling frequency using the WinWCP software (Strathclyde University, UK) driving an AD converter (National Instruments, USA).

Swimming performance assays and oxygen consumption measurements

Swimming performance tests and oxygen consumption measurements were performed as previously described [45]. The detailed procedure and measurements are detailed in Supplementary Material and Methods. Videos were acquired during swimming step protocol experiments, at a moderate (5BL.s^{-1}) and quite rapid (8 BL.s^{-1}) water flow respectively. Movies are played 10 times slower than original speed. Biometry of the fish used for these experiments is shown in (supplement Table 3). Swimming performance assays was performed in both lines and oxygen consumption was only measured in *col22a1*$^{TSPN-/-}$. Live 2wpf larvae were placed in Danieau media. The motility of larvae was recorded using a Zeiss Axiozoom V16 stereoscopic microscope with a high resolution AxioCam HRm Rev.3 Firewire camera. To assess swimming activity of the fish, video-recorded at 5 ms/frame, during 25s was performed without any stimulation. Videos of 6mpf zebrafish were recorded using a high-speed camera MiroM310.

Statistical analysis

Statistical analyses were carried out using GraphPad Prism or XRealSats' Excel macro software. Depending on the experiments, the statistical methods to compare datasets were different and include one-way ANOVA, Kruskal-Wallis test, Student's t-test and Mann-Whitney U test. The statistical method is indicated in the legend of the Figures.

Acknowledgments: We thank Prof Manuel Koch (University of Cologne) and Dr Loïc Teulier (LENHA, Lyon) for helpful discussion. We are deeply grateful for the assistance of Sophie Gilardeau for statistical analysis. We acknowledge Robert Renard for his assistance with the swimming tunnel implementation, Cherif Kabir for his helpful IT assistance with the swimming tunnel software, Loup Plantevin (INSA, Lyon) for his kind help with swimming tunnel calibration. We thank the 'Centre Technique des Microstructures' (UCBL, Villeurbanne) for technical assistance with transmission electron microscopy.

Funding: This work was supported by the CNRS and the "Association Française contre les Myopathies" [MNM1-2010] to FR. AG is a recipient of a post-doc fellowship from the "Association Française contre les Myopathies". PN is a recipient of the French government (NMRT) and the "Fondation pour la Recherche Médicale" (FDT20160435169) fellowships.

References

[1] D.I. Bassett, Dystrophin is required for the formation of stable muscle attachments in the zebrafish embryo, Development 130 (2003), 5851–5860.

[2] R. Postel, P. Vakeel, J. Topczewski, R. Knöll and J. Bakkers, Zebrafish integrin-linked kinase is required in skeletal muscles for strengthening the integrin-ECM adhesion complex. Dev. Biol. 318 (2008), 92–101.

[3] T.E. Hall, R.J. Bryson-Richardson, S. Berger, A.S. Jacoby, N.J. Cole, G.E. Hollway, J. Berger, and P.D. Currie, The zebrafish candyfloss mutant implicates extracellular matrix adhesion failure in laminin 2-deficient congenital muscular dystrophy. Proc. Natl. Acad. Sci. 104 (2007), 7092–7097.

[4] D.J. Law and J.G. Tidball, Dystrophin deficiency is associated with myotendinous junction defects in prenecrotic and fully regenerated skeletal muscle. Am. J. Pathol. 142 (1993), 1513–1523.

[5] D.J. Law, A. Caputo, and J.G. Tidball, Site and mechanics of failure in normal and dystrophin deficient skeletal muscle. Muscle Nerve 18 (1995), 216–223.

[6] J. Desaki, Scanning electron microscopical study of skeletal muscle fiber ends in normal and dystrophic mice. Arch. Histol. Cytol. 55(4) (1992), 449-452.

[7] N. Miosge, C. Klenczar, R. Herken, M. Willem, and U. Mayer, Organization of the myotendinous junction is dependent on the presence of alpha7beta1 integrin. Lab Invest 79 (1999), 1591–1599.

[8] J. V. Welser, J.E. Rooney, N.C. Cohen, P.B. Gurpur, C.A. Singer, R.A. Evans, B.A. Haines, and D.J. Burkin, Myotendinous junction defects and reduced force transmission in mice that lack α7 integrin and utrophin. Am. J. Pathol. 175 (2009), 1545–1554.

[9] P.W. Ingham, The power of the zebrafish for disease analysis. Hum. Mol. Genet. 18 (2009), 107–112.

[10] T.E. Sztal, C. Sonntag, T.E. Hall, and P.D. Currie, Epistatic dissection oflaminin-receptor interactions in dystrophic zebrafish muscle. Hum. Mol. Genet. 21 (2012), 4718–4731).

[11] B. Charvet, A. Guiraud, M. Malbouyres, D. Zwolanek, E. Guillon, S. Bretaud, C. Monnot, J. Schulze, H.L. Bader, B. Allard, Knockdown of col22a1 gene in zebrafish induces a muscular dystrophy by disruption of the myotendinous junction. Development 140 (2013), 4602–4613.

[12] A. Subramanian and T.F. Schilling, Thrombospondin-4 controls matrix assembly during development and repair of myotendinous junction. Elife. 18 (2014); 3:e02372.

[13] M. Koch, J. Schulze, U. Hansen, T. Ashwodt, D.R. Keene, W.J. Brunken, R.E. Burgeson, P. Bruckner and L. Bruckner-Tuderman, A novel marker of tissue junctions, collagen XXII. J. Biol. Chem. 279 (2004), 22514–22521.

[14] K.R. Jacobson, S. Lipp, A. Acuna, Y. Leng, Y. Bu and S. Calve, Comparative Analysis of the Extracellular Matrix Proteome across the Myotendinous Junction. J. Proteome Res. 2 (2020),19(10), 3955-3967.

[15] M.J. Petrany, C.O. Swoboda, C. Sun, K. Chetal, X. Chen, M.T. Weirauch, N. Salomonis, and D.P. Millary, Single-nucleus RNA-seq identifies transcriptional heterogeneity in multinucleated skeletal myofibers. Nat. Commun. 11(1) (2020), 6374.

[16] E. Miyamoto-Mikami, H. Kumagai, N. Kikuchi, N. Kamiya, N. Miyamoto, and N. Fuku, eQTL variants in COL22A1 are associated with muscle injury in athletes. Physiol. Genomics. 1, 52(12) (2020), 588-589.

[17] S. Schulte-Merker and D.Y.R. Stainier, Out with the old, in with the new: reassessing morpholino knockdowns in light of genome editing technology. Development 141 (2014), 3103–3104.

[18] F.O. Kok, M. Shin, C-W. Ni, A. Gupta, A.S. Grosse, A. van Impel, B.C. Kirchmaier, J. Peterson-Maduro, G. Kourkoulis, I. Male, D.F. DeSantis, S. Sheppard-Tindell, L. Ebarasi, C. Betsholtz, S. Schulte-Merker, S.A. Wolfe, and N.D. Lawson, Reverse genetic screening reveals poor correlation between Morpholino-induced and mutant phenotypes in zebrafish. Dev. Cell. 32(1) (2015), 97-108.

[19] M.A. El-Brolosy and D.Y.R. Stainier, Genetic compensation: A phenomenon in search of mechanisms. PLoS Genet. 13 (2017), 1–17.

[20] J. Chelly and I. Desguerre, Progressive muscular dystrophies. Handb. Clin. Neurol. 113 (2013), 1343-1346.

[21] H.L. Bader, D.R. Keene, B. Charvet, G. Veit, W. Driever, M. Koch and F. Ruggiero, Zebrafish collagen XII is present in embryonic connective tissue sheaths (fascia) and basement membranes. Matrix Biol. 28 (2009), 32–43.

[22] H.L. Bader, E. Lambert, A. Guiraud, M. Malbouyres, W. Driever, M. Koch, and F. Ruggiero, Zebrafish collagen XIV is transiently expressed in epithelia and is required for proper function of certain basement membranes. J. Biol. Chem. 288 (2013), 6777–6787.

[23] P. Nauroy, S. Hughes, A. Naba, and F. Ruggiero, The in-silico zebrafish matrisome: A new tool to study extracellular matrix gene and protein functions. Matrix Biol. 65 (2018), 5–13.

[24] P. Nauroy, A. Guiraud, J. Chlasta, M. Malbouyres, B. Gillet, S. Hughes, E. Lambert and F. Ruggiero, Gene profile of zebrafish fin regeneration offers clues to kinetics, organization and biomechanics of basement membrane. Matrix. Biol. 75-76 (2019), 82-101.

[25] S. Glasauer and H. Straka, Postural control: learning to balance is a question of timing. Curr. Biol. 27(3) (2017):105-107.

[26] D.E. Ehrlich and D. Schoppik, Control of Movement Initiation Underlies the Development of Balance. Curr. Biol. 6 (2017), 27(3), 334-344.

[27] C. Hammer, Fatigue and exercise tests with fish. Comp. Biochem. Physiol. Part A Physiol. 112 (1995), 1–20.

[28] T. Groennebaek and K. Vissing, Impact of Resistance Training on Skeletal Muscle Mitochondrial Biogenesis, Content, and Function. Front. Physiol., 15 (2017), 8, 713.

[29] C. Lundby and R.A. Jacobs, Adaptations of skeletal muscle mitochondria to exercise training. Exp. Physiol. 101(1) (2016), 17-22.

[30] J.R. Jakobsen and M.R. Krogsgaard, The Myotendinous Junction-A Vulnerable Companion in Sports. A Narrative Review. Front. Physiol. 26 (2021), 12, 635561.

[31] N.D. Lawson, Reverse Genetics in Zebrafish: Mutants, Morphants, and Moving Forward. Trends Cell. Biol. 26(2) (2016), 77-79.

[32] A.S. Jacoby, E. Busch-Nentwich, R.J. Bryson-Richardson, T.E. Hall, J. Berger, S. Berger,

C. Sonntag, C. Sachs, R. Geisler, D.L. Stemple, The zebrafish dystrophic mutant softy maintains muscle fibre viability despite basement membrane rupture and muscle detachment. Development 136 (2009), 3367–3376.

[33] D.A. Hood, L.D. Tryon, H.N. Carter, Y. Kim, and C.C. Chen, Unravelling the mechanisms regulating muscle mitochondrial biogenesis. Biochem. J. 473(15) (2016), 2295-314.

[34]. R. Ferreira, R. Vitorino, R.M.P. Alves, H.J Appell and S.K. Powers, Subsarcolemmal and intermyofibrillar mitochondria proteome differences disclose functional specializations in skeletal muscle. Proteomics. 10(17) (2010), 3142-54.

[35] R. Pereira, K. Halford, B.P. Sokolov, J.S. Khillan and D.J. Prockop, Phenotypic variability and incomplete penetrance of spontaneous fractures in an inbred strain of transgenic mice expressing a mutated collagen gene (COL1A1). Clinical Investigation. 93 (1994), 1765.

[36] C. Jin, K. Yao, J. Jiang, X. Tang, X. Shentu, and R. Wu, Novel *FBN1* mutations associated with predominant ectopia lentis and marfanoid habitus in Chinese patients. Molecular Vision. 13 (2007), 1280–1284.

[37] D. Li, J. Yu, F. Gu, X. Pang, X. Ma, R. Li, N. Liu and X. Ma, The roles of two novel FBN1 gene mutations in the genotype-phenotype correlations of Marfan syndrome and ectopia lentis patients with marfanoid habitus. Genetic Testing. 12 (2008), 325–330.

[38] I. Lobo, Same Genetic Mutation, Different Genetic Disease Phenotype. Nature Education. 1(1) (2008): 64.

[39] Z. Kontarakis and D.Y.R. Stainier, Genetics in Light of Transcriptional Adaptation. Trends Genet. 36(12) (2020), 926-935.

[40] A. Rossi, Z. Kontarakis, C. Gerri, H. Nolte, S. Hölper, M. Krüger, and D.Y.R. Stainier, Genetic compensation induced by deleterious mutations but not gene knockdowns. Nature 524 (2015), 230–233.

[41] J. Fitzgerald, and J.F. Bateman, Why mice have lost genes for COL21A1, STK17A, GPR145 and AHRI: evidence for gene deletion at evolutionary breakpoints in the rodent lineage. Trends in Genetics. 20(9) (2004), 408-412.

[42] V. Léjard, G. Brideau; F. Blais; R. Salingcarnboriboon; G. Wagner; M.H.A. Roehrl, M. Noda; D. Duprez; P. Houillier and J. Rossert, Scleraxis and NFATc Regulate the Expression of the Pro-α1(I) Collagen Gene in Tendon Fibroblasts. J. Biol. Chem. 282 (24) (2007), 17665-17675.

[43] K.M.T.H. Rahit and M. Tarailo-Graovac, Genetic Modifiers and Rare Mendelian Disease. Genes (Basel). 11(3) (2020), 239.

[44] J.C. Talbot and S.L. Amacher, A Streamlined CRISPR Pipeline to Reliably Generate Zebrafish Frameshifting Alleles. Zebrafish 11 (2014), 583–585.

[45] J. Lucas, I. Percelay, T. Larcher and C. Lefrançois, Effects of pyrolytic and petrogenic polycyclic aromatic hydrocarbons on swimming and metabolic performance of zebrafish contaminated by ingestion. Ecotoxicol. Environ. Saf. 132 (2016), 145–152.

Figure legends

Figure 1: Generation and validation of *col22a1 knockout zebrafish lines.* A. Upper panel. Generation of the CRISPR/Cas9-mediated *col22a1* knockout zebrafish lines, *col22a1^{vWA}* and *col22a1^{TSPN}.* Schematic representation of the targeted *col22a1* regions in *col22a1* exon 2 (*col22a1^{vWA}* line) and exon 6 (*col22a1^{TSPN}* line). For each exon, the upper sequence corresponds to the WT sequence containing the sgRNA-targeted nucleotides (underlined) followed by the PAM sequence (in red). The lower sequence corresponds to the resulting 8 nucleotides and 4 nucleotides deletions in exon 2 (*col22a1^{vWA}* line) and exon 6 (*col22a1^{TSPN}* line), respectively. Each deleted nucleotide is represented by a space. Lower panel shows the zebrafish collagen XXII (ColXXII) primary structure. At the N-terminus, the VWA and TSPN domains represent the building blocks of the NC6 domain. COL1-COL5, collagenous domains, NC1-6, non-collagenous domains. Red bars are short interruptions in COL1. In contrast to humans, zebrafish ColXXII lacks a NC4 domain (resulting in a fused COL3-COL4 domain). Y (in red) points to the recombinant domain used to generate antibodies to ColXXII (Charvet el al, 2013). Black arrows indicate the predicted truncation of ColXXII resulting from premature codon stop in exon 2 (*col22a1^{vWA}* line) and exon 6 (*col22a1^{TSPN}* line) domains. B. Whole-mount immunofluorescence staining of 5dpf WT (left), *col22a1$^{TSPN-/-}$* (middle) and *col22a1$^{vWA-/-}$* (right) with anti-ColXXII (red) and the myoseptal marker anti-ColXII (green) as positive control. The upper cartoon shows orientation of the larvae, the red box indicates the region imaged in WT, *col22a1$^{TSPN-/-}$* and *col22a1$^{vWA-/-}$* larvae.

Figure 2: ***col22a1* knockout-associated *phenotypic classes***. A. Representative bright field images of 5 dpf, 2 wpf and 6 mpf *col22a1$^{TSPN-/-}$* and WT individuals. *col22a1$^{-/-}$* class 2 larvae can be identified at around 2 wpf based on their posture defect and altered swimming capacity compared to WT. Arrows point to the empty gut observed only in 2 wpf *col22a1$^{TSPN-/-}$* class 2 fish. Values (in mm) are the total body length of individual fish. B. Quantification of the total body length of 5dpf *col22a1$^{TSPN-/-}$* larvae (grey bars), 2 wpf and 6mpf class 1 (blue bars) and class 2 (red bars) *col22a1$^{TSPN-/-}$* fish and WT (black bars). Statistical analysis was performed

using a Kruskal-Wallis followed by Dunn's post hoc test (for 2wpf fish) and a Mann-Whitney U test (for 5dpf and 6mpf fish). Data are mean ± SD. ***p<0.001; *p<0.05; ns, not significant. n = number of larvae for each group. C. Real time RT-PCR analysis of *col22a1* gene expression in 2 wpf class 1 (blue bars) and class 2 (red bars) *col22a1*$^{TSPN-/-}$ fish and WT (black bars). Different primers have been designed to amplify specific sequences in the TSPN, vWA and COL5 domains respectively as indicated into brackets. Data were normalized to *polr2d*. Levels of *col22a1* expression were compared to WT expression, which was arbitrary set to 1. Statistical analysis was performed using a one-way ANOVA and tukey's post-hoc tests. Data are mean ± SEM (n=3). ****p<0.0001; ***p<0.001; ns, not significant.

Figure 3: **Muscle contractile performance and myotendinous unit ultrastructure of2wpf mutant larvae.** A. Representative twitch responses (upper traces) elicited by single supramaximal electric shocks of 0.5 ms duration (lower trace) in *col22a1*$^{TSPN-/-}$ class 1 (blue), class 2 (red), *col22a1*$^{TSPN+/-}$ (orange) and wild-type (black) larvae (left panel) and histograms showing mean twitch amplitudes in different fish lines (right panel). B. Representative tetanic force (upper traces) recorded in response to trains of 0.5 ms duration electric shocks delivered at a frequency of 50 Hz during 250 ms (lower trace) (left panel) and histograms showing mean amplitude of tetanic force in different fish lines (right panel). Statistical analysis was performed using a Kruskal-Wallis and Dunn's post hoc tests. Data are mean ± SEM. ***p<0,001; **p<0,01; ns, not significant. n = number of analyzed larvae for each group. C. Transmission electron microscopy (TEM) representative images of the trunk skeletal muscle (upper panel) and of the myotendinous region (lower panel) of class 1 and class 2 *col22a1*$^{TSPN-/-}$ and WT larvae. Arrows point to distended myosepta that contain sparse bundles of collagen fibrils (Cf) of lucent electron density. Arrowheads point to MTJ. Asterisks indicate the characteristic zigzag morphology of the MTJ in WT. Red lines on the left delineate the MTJ in WT and *col22a1*$^{TSPN-/-}$ skeletal muscle. All images are longitudinal sections of the trunk muscle. Cf, Collagen fibers; f, fibroblast; ms, vertical myosepta. Scale bars = 0.5µm. D. Quantification of the sarcolemmal folds at the MTJ. Measurements were performed on TEM images of different areas of trunk

muscle per larva at the same magnification using ImageJ software. The values are expressed as a total length of sarcolemma at the MTJ level (as exemplified with red lines in C) per 100 μM^2 of muscle tissue of class 1 and class 2 *col22a1*$^{TSPN-/-}$ and WT larvae (the total area analyzed for each group is >1950μm^2). Statistical analysis was performed using Kruskal-Wallis and Dunn's post-hoc tests. Data are mean ± SEM. ***p<0.001; ns, not significant.

Figure 4: Structural analysis of 5 dpf *col22a1*$^{TSPN-/-}$ trunk muscle. A. Representative bright field images of *col22a1*$^{TSPN-/-}$ and wildtype (WT) larvae before (upper, unstimulated) and after repeated electric stimulation (lower, stimulated). Arrows point to abnormally wavy muscle fibers. B. Birefringence images of *col22a1*$^{TSPN-/-}$ and WT larvae before (upper, unstimulated) and after (lower, stimulated) repeated electric stimulations. Quantification of birefringence (bottom panel). Data were analyzed using one-way ANOVA and showed no statistical difference between the groups; n=10 for each group. C. Whole-mount immunofluorescence staining with antibodies against ColXXII (green) and the myosin light chain 1 marker (F310, red). Nuclei are in blue. Anterior is towards the left.

Figure 5: Dysregulation of the MTJ gene expression in *col22a1*$^{-/-}$ mutants. A. Schematic representation of the 2 transmembrane linkage systems enriched at the MTJ, the dystroglycan-glycoprotein complex (DGC) (left) and $\alpha 7\beta 1$ integrin complex (right). The presumptive location of ColXXII as part of the $\alpha 7\beta 1$ integrin complex is illustrated. B. Real time RT-PCR analysis of selected gene expression in 2 wpf trunk RNA extracts from *col22a1*$^{TSPN-/-}$ class 1 (blue) and class 2 (red) sibblings and WT (black). Data were normalized to *polr2d*. The expression levels of the different genes were compared to WT expression, which was arbitrary set to 1. Statistical analysis was performed using a one-way ANOVA followed by Tukey's post hoc test. Data are mean ± SEM (n=3). ****p<0.0001; ***p<0.001; **p<0.01; *p<0.05; ns, not significant.

Figure 6: **Postural and swimming behaviors of col22a1 mutants**. Single frame from representative movies of 2wpf *col22a1*$^{TSPN-/-}$ (A) and *col22a1*$^{vWa-/-}$ (B) larvae. Row 1 shows WT

sibling as control, row 2 and row 3 show class 1 and class 2 larvae respectively. t, time expressed in seconds (s). n= number of analyzed larvae; wpf, weeks post-fertilization.

Figure 7: Muscle performance assays of 6 mpf *col22a1*$^{TSPN-/-}$ class 1 fish. A Flowchart of the experimental swimming step protocol tested in the swimming tunnel respirometer. B. Representative capture images of challenged *col22a1*$^{TSPN-/-}$ mutants (fish #1: 4,5,6 and #2: 7,8,9) and wildtype (WT: 1,2,3) fish at different swimming speed: 5BLs^{-1} (1,4,7), 6.5BLs^{-1} (2,5,8) and 8BLs^{-1} (3,6,9). C Mean of critical swimming speed (U_{crit}) values of (left) *col22a1*$^{TSPN-/-}$ mutants (grey bar) and WT (black bar); (right) *col22a1*$^{vWA-/-}$ mutants (grey bar) and WT (black bar). BLs^{-1}, body length per second. Statistical analysis was performed using a two-tailed Student t-test. Data are mean ± SEM. ***p_value<0.001; **p<0.01.

Figure 8: **Oxygen consumption and ultrastructure of myotendinous unit of 6 mpf *col22a1*$^{TSPN-/-}$ class 1 fish.** A. Measurements of oxygen consumption (MO2) during the step protocol of *col22a1*$^{TSPN-/-}$ (grey diamond) and WT (black square) fish. n, number of fish analyzed. Data are mean ± SD, n = number of fish. Statistical analysis was performed using a two-tailed Student's t-test for paired samples (p_value= 0.00005). B. Representative TEM images of the trunk muscle of WT (upper panel) and class 1 *col22a1*$^{TSPN-/-}$ (lower panel) fish. Upper panel: arrows point to MTJ interdigitations. Lower panel: arrows indicate IMF mitochondria. Cf, Collagen fibers; fb, fibroblast; mf, myofibrils; ms, myosepta; ssm, subsarcolemmal mitochondria. C. Distribution of IMF (left, number of IMFs) and SSM (right, SSM density) in WT and *col22a1*$^{TSPN-/-}$ unchallenged fish. For SSM, the percentage of muscle fibers occupied by the mitochondria was measured with imageJ software. The total area analyzed for each group (n=3 fish) is >11,000 µm2 for IMF and >3,280 µm^2 for SSM. Statistical analysis was performed using a Mann-Whitney U test (for IMF and SS). Data are mean ± SEM.

***p_value<0.001; ns, not significant.

Table 1: **Variable expressivity of *col22a1*$^{vWA-/-}$ and *col22a1*$^{TSPN-/-}$ larval phenotypes at 2wpf**

Genotype	Generation	Number of embryos	Larval phenotype (%)			Premature mortality rate (%) (before 4dpf)
			Wildtype	Class 1	Class 2	
WT	F4	214	96.73	-	-	3.27
WT	F5	225	98.22	-	-	1.78
WT	F6	343	97.08	-	-	2.92
col22a1$^{vWA-/-}$	F5 (1)	88	-	67.05	31.82	1.13
col22a1$^{vWA-/-}$	F5 (2)	113	-	74.34	23.89	1.77
col22a1$^{vWA-/-}$	F6	84	-	67.86	29.76	2.38
col22a1$^{TSPN-/-}$	F5 (1)	109	-	68.81	29.36	1.83
col22a1$^{TSPN-/-}$	F5 (2)	141	-	72.34	25.53	2.13
col22a1$^{TSPN-/-}$	F6	90	-	63.33	35.56	1.11

The severity of the phenotype is scored as swimming capacity and posture impairment using a stereoscope. dpf, days post-fertilization. Numbers into brackets indicate that different laying from F5 fish were used.

Figure 1

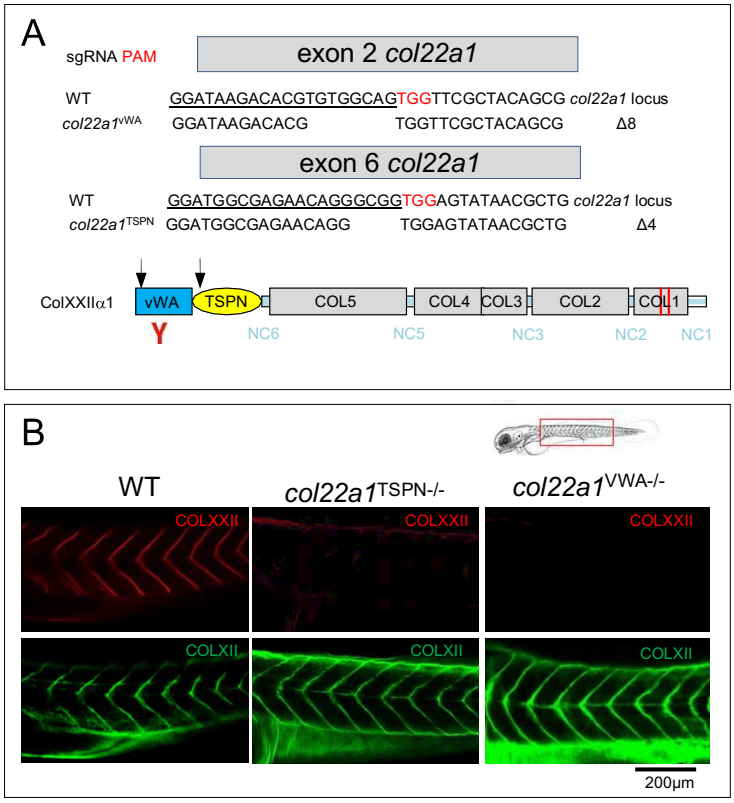
A
sgRNA PAM
exon 2 col22a1
WT GGATAAGACACGTGTGGCAGTGGTTCGCTACAGCG col22a1 locus
col22a1VWA GGATAAGACACG TGGTTCGCTACAGCG Δ8
exon 6 col22a1
WT GGATGGCGAGAACAGGGCGGTGGAGTATAACGCTG col22a1 locus
col22a1TSPN GGATGGCGAGAACAGG TGGAGTATAACGCTG Δ4
ColXXIIα1
vWA
TSPN
COL5
COL4
COL3
COL2
COL1
NC6
NC5
NC3
NC2
NC1
B
WT
col22a1TSPN-/-
col22a1VWA-/-
COLXXII
COLXII
200μm

Figure 2

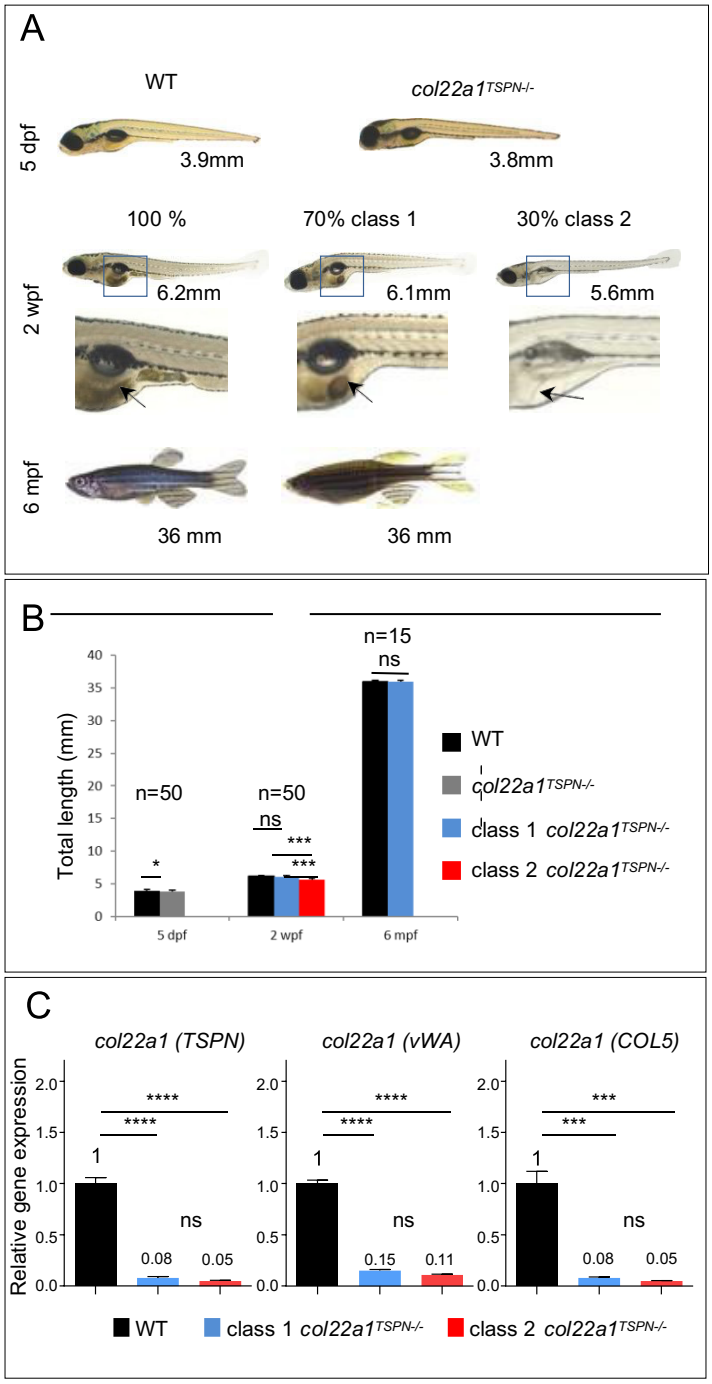
A
WT
col22a1TSPN-/-
5 dpf
3.9mm
3.8mm
100 %
70% class 1
30% class 2
2 wpf
6.2mm
6.1mm
5.6mm
6 mpf
36 mm
36 mm
B
Total length (mm)
n=50
n=50
ns
n=15
ns
***
***
*
5 dpf
2 wpf
6 mpf
WT
col22a1TSPN-/-
class 1 col22a1TSPN-/-
class 2 col22a1TSPN-/-
C
col22a1 (TSPN)
col22a1 (vWA)
col22a1 (COL5)
Relative gene expression
****
****
***
1
ns
0.08
0.05
0.15
0.11
WT
class 1 col22a1TSPN-/-
class 2 col22a1TSPN-/-

Figure 3

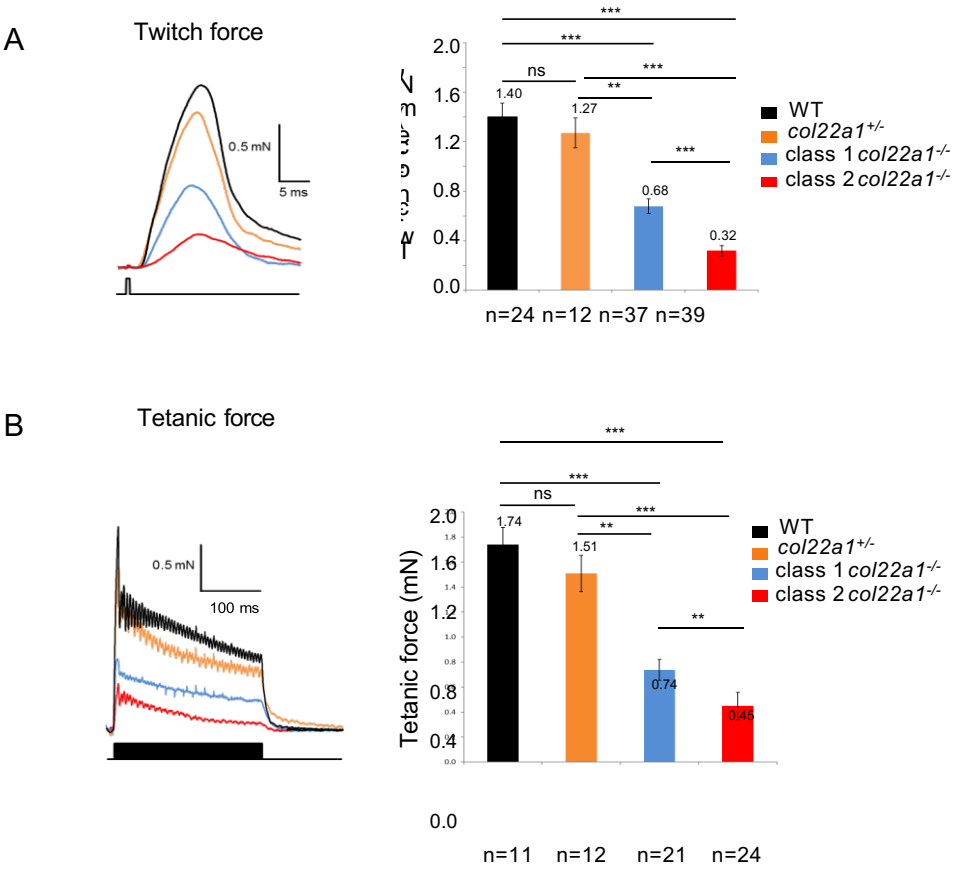
A
Twitch force
0.5 mN
5 ms
Twitch force (mN)
2.0
1.6
1.2
0.8
0.4
0.0
***
***
ns
***
**
***
1.40
1.27
0.68
0.32
n=24 n=12 n=37 n=39
WT
col22a1+/-
class 1 col22a1-/-
class 2 col22a1-/-
B
Tetanic force
0.5 mN
100 ms
Tetanic force (mN)
2.0
1.6
1.2
0.8
0.4
0.0
***
***
ns
***
**
**
1.74
1.51
0.74
0.45
n=11 n=12 n=21 n=24
WT
col22a1+/-
class 1 col22a1-/-
class 2 col22a1-/-

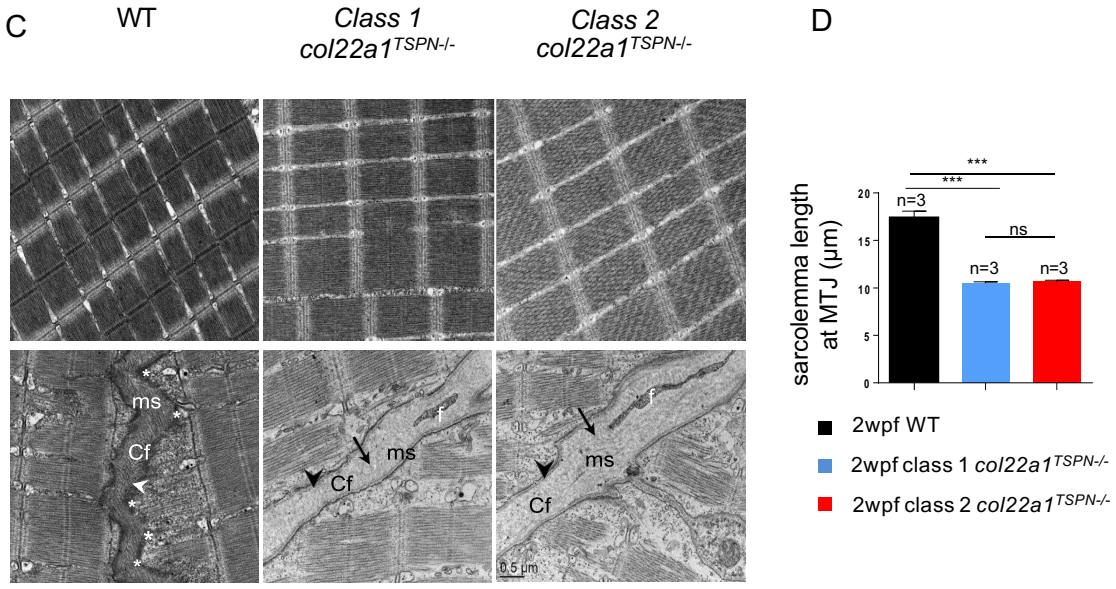
C
WT
Class 1
col22a1TSPN-/-
Class 2
col22a1TSPN-/-
ms
Cf
ms
Cf
ms
Cf
0.5 µm
D
sarcolemma length at MTJ (µm)
20
15
10
5
0
***
***
ns
n=3
n=3
n=3
2wpf WT
2wpf class 1 col22a1TSPN-/-
2wpf class 2 col22a1TSPN-/-

Figure 4

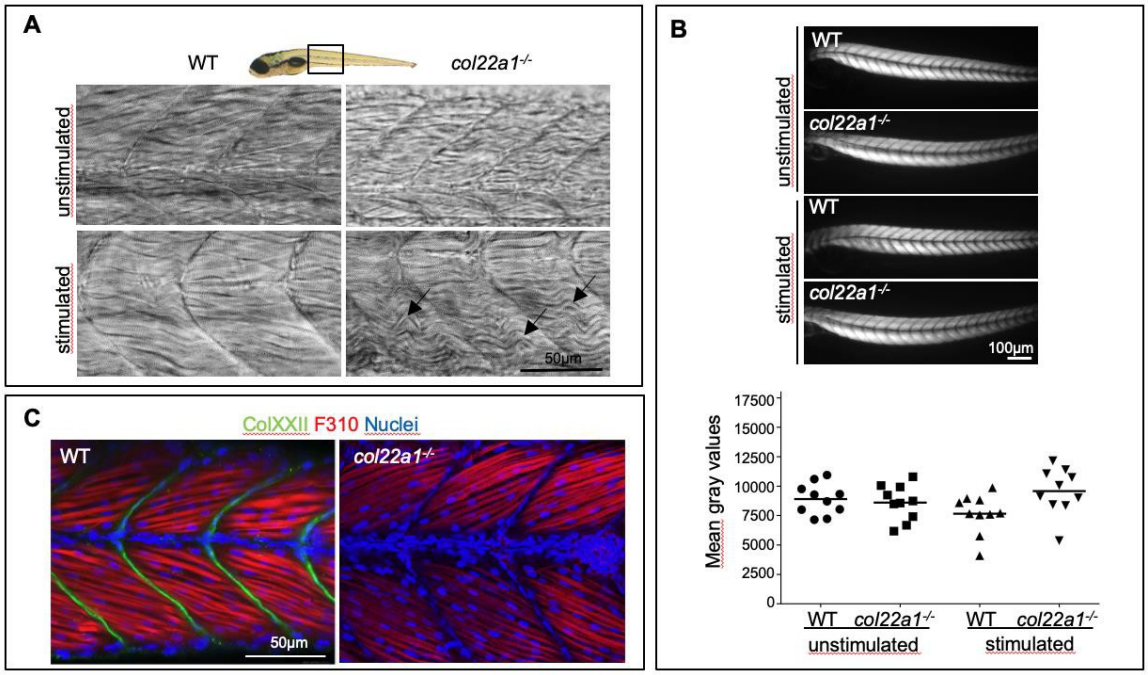
A
WT
col22a1-/-
unstimulated
stimulated
50µm
B
WT
col22a1-/-
unstimulated
WT
col22a1-/-
stimulated
100µm
Mean gray values
17500
15000
12500
10000
7500
5000
2500
0
WT col22a1-/-
unstimulated
WT col22a1-/-
stimulated
C
ColXXII F310 Nuclei
WT
col22a1-/-
50µm

Figure 5

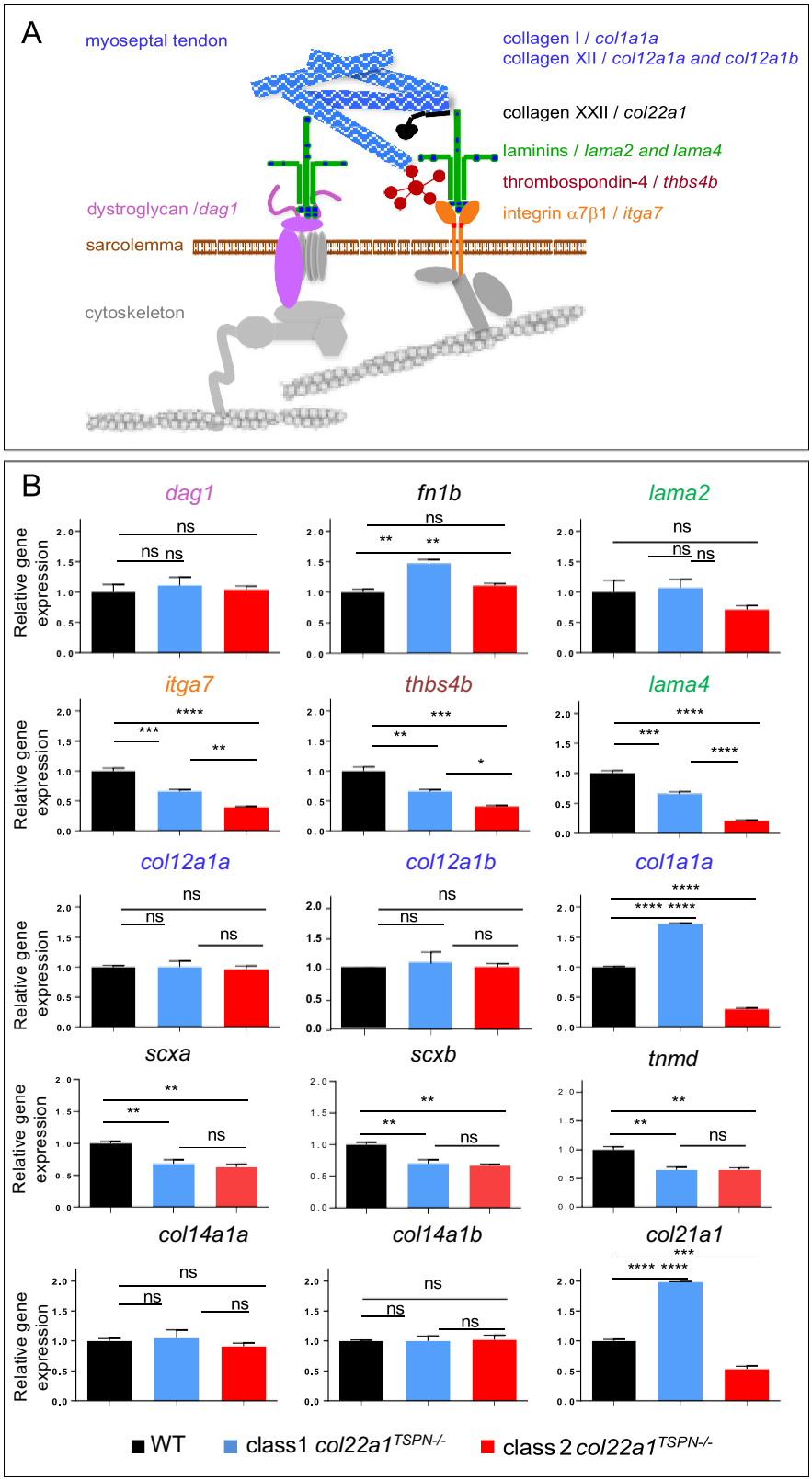
A
myoseptal tendon
collagen I / col1a1a
collagen XII / col12a1a and col12a1b
collagen XXII / col22a1
laminins / lama2 and lama4
thrombospondin-4 / thbs4b
integrin α7β1 / itga7
dystroglycan /dag1
sarcolemma
cytoskeleton
B
dag1
fn1b
lama2
itga7
thbs4b
lama4
col12a1a
col12a1b
col1a1a
scxa
scxb
tnmd
col14a1a
col14a1b
col21a1
Relative gene expression
WT
class1 col22a1TSPN-/-
class 2 col22a1TSPN-/-

Figure 6

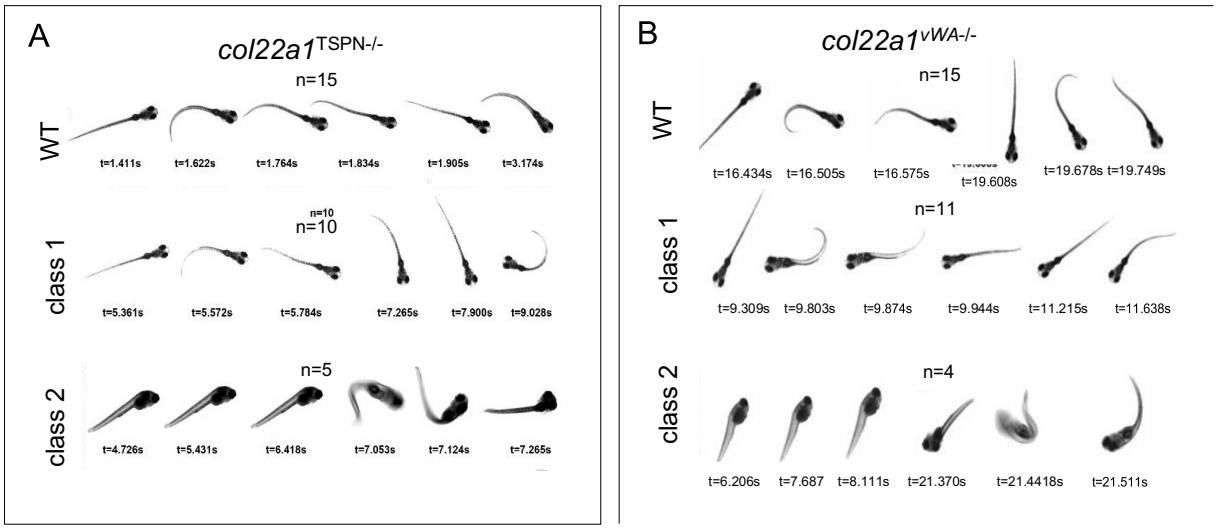
A
col22a1TSPN-/-
n=15
WT
t=1.411s
t=1.622s
t=1.764s
t=1.834s
t=1.905s
t=3.174s
n=10
n=10
class 1
t=5.361s
t=5.572s
t=5.784s
t=7.265s
t=7.900s
t=9.028s
n=5
class 2
t=4.726s
t=5.431s
t=6.418s
t=7.053s
t=7.124s
t=7.265s
B
col22a1vWA-/-
n=15
WT
t=16.434s
t=16.505s
t=16.575s
t=19.608s
t=19.678s
t=19.749s
n=11
class 1
t=9.309s
t=9.803s
t=9.874s
t=9.944s
t=11.215s
t=11.638s
n=4
class 2
t=6.206s
t=7.687
t=8.111s
t=21.370s
t=21.4418s
t=21.511s

Figure 7

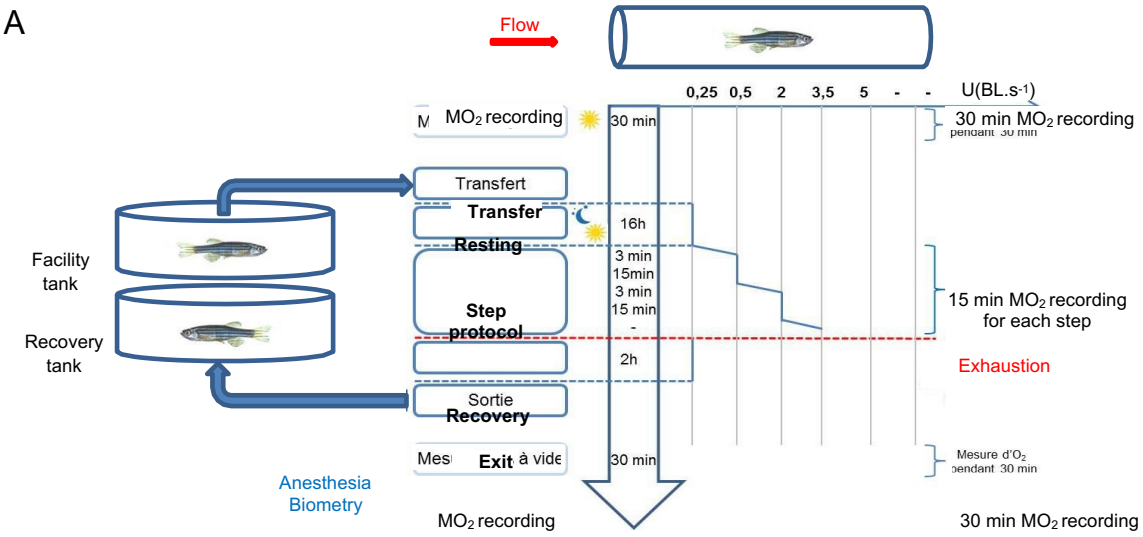
A
Flow
0,25 0,5 2 3,5 5 - - U(BL.s-1)
MO2 recording
30 min
30 min MO2 recording
Transfert
Transfer
Resting
16h
3 min
15min
3 min
15 min
-
15 min MO2 recording
for each step
Facility
tank
Recovery
tank
Step
protocol
2h
Exhaustion
Sortie
Recovery
Exit à vide
30 min
Anesthesia
Biometry
MO2 recording
30 min MO2 recording

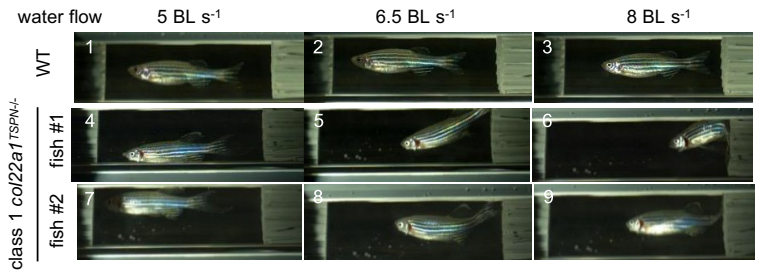
B
water flow
5 BL s-1
6.5 BL s-1
8 BL s-1
WT
class 1 col22a1TSPN-/-
fish #1
fish #2
1
2
3
4
5
6
7
8
9

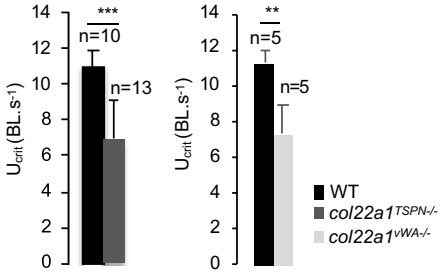
C
Ucrit (BL.s-1)
***
n=10
n=13
**
n=5
n=5
WT
col22a1TSPN-/-
col22a1vWA-/-

Figure 8

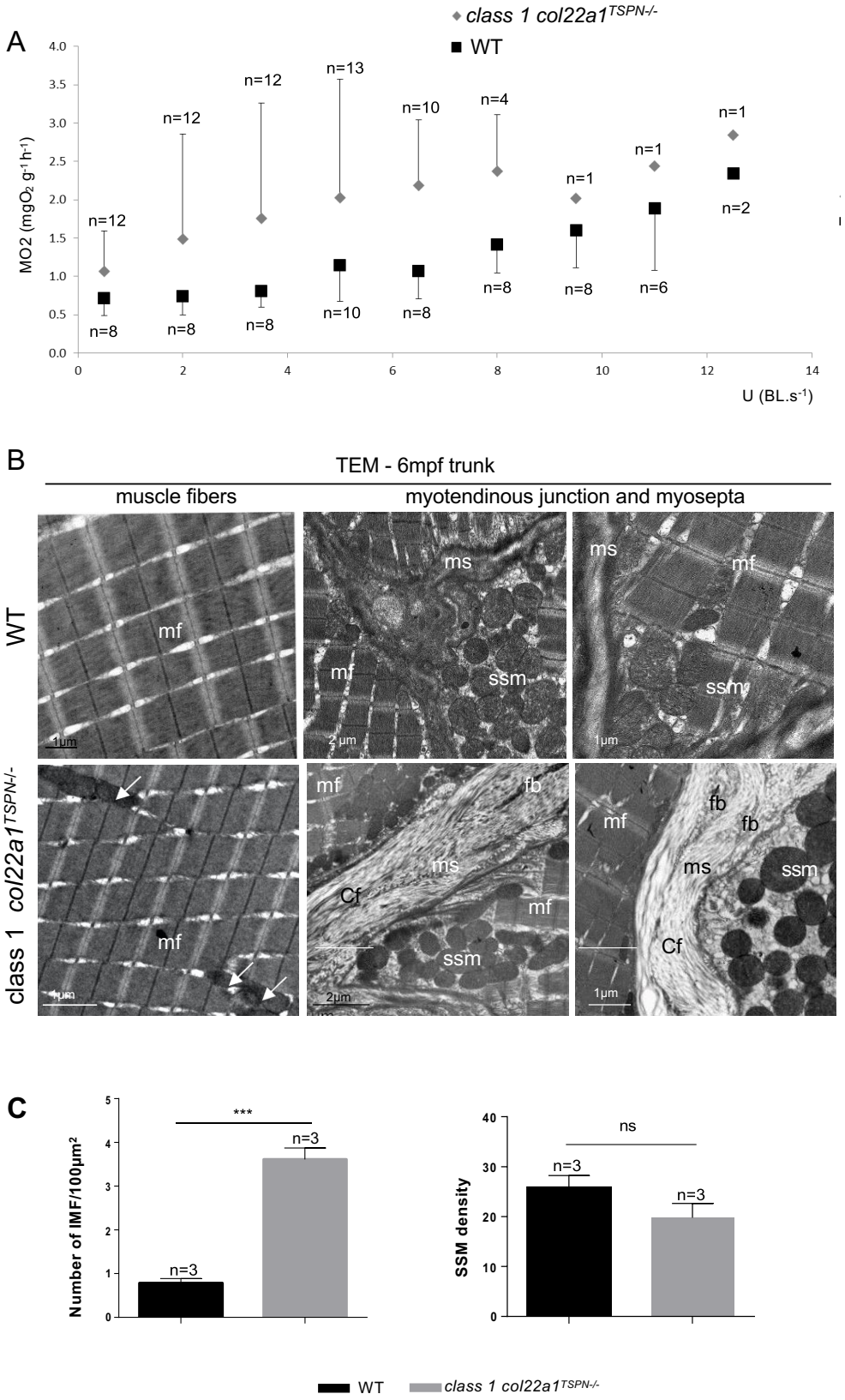
A
class 1 col22a1TSPN-/-
WT
MO2 (mgO2 g-1 h-1)
U (BL.s-1)
n=12
n=8
n=12
n=8
n=12
n=8
n=13
n=10
n=10
n=8
n=4
n=8
n=1
n=8
n=1
n=6
n=1
n=2
B
TEM - 6mpf trunk
muscle fibers
myotendinous junction and myosepta
WT
class 1 col22a1TSPN-/-
mf
ms
ssm
fb
Cf
1µm
2µm
C
Number of IMF/100µm²
***
n=3
n=3
SSM density
ns
n=3
n=3
WT
class 1 col22a1TSPN-/-

Supplementary Materials and Methods

Swimming performance tests and oxygen consumption measurements

Swimming performance tests and oxygen consumption measurements were performed as previously described (Lucas et al., 2016). Critical swimming speed (i.e. the maximal velocity a fish can reach during a swimming step protocol, U_{crit}; Hammer, 1995) is frequently employed as an indicator of swimming capacities. Since U_{crit} notably depends on the maximal ability of fish to provide energy during sustained swimming activity, these studies are often associated with the assessment of metabolic performance. Aerobic metabolic scope (AMS; Brett, 1964; Fry, 1971) is defined as the difference between the active metabolic rate (AMR), which is the highest metabolic rate the organism can sustain under maximal activity and the standard metabolic rate (SMR), the metabolic rate necessary to maintain vital functions and measured under resting conditions.

Experimental set-up - Two identical 170 mL swimming respirometers (Loligo Systems, Denmark) were used to assess the swimming and metabolic performance of fish. Each swimming respirometer was composed of (a) a swimming chamber, where the fish was placed to be tested, (b) a motor fitted with a three-bladed propeller to control water flow and (c) honeycomb placed at each side of the swimming chamber to laminarize the water flow. Each swimming respirometer was submerged in a 20 L buffer tank, and filled with temperature controlled (i.e. 28°C) and oxygenated mixed water as in the rearing system.

The oxygen consumption (MO_2 in mg O_2 $g^{-1}h^{-1}$) associated with the activity of fish was measured by intermittent flow respirometry. Water supply in each swimming respirometer was provided by flush pumps, which controlled water flow from the buffer tank to the swimming respirometer. This allowed alternation between phases of oxygen renewal and phases of MO_2 measurement with a cycle of 3: 15 min. An oxygen probe (fibre optic sensor, PreSens, Germany) was used to record oxygen concentration in the swimming respirometer where the fish was placed. The probe was connected to a multichannel oxygen measuring system (OXY 4 mini, PreSens, Germany) to record the level of dissolved oxygen in the water every 5 s. Optic fibers was calibrated once at the beginning of the swim test using 0% and 100% air saturation for a controlled temperature of 28°C. A conversion factor based on oxygen solubility into water was used to convert oxygen data from per cent saturation to mgO_2L^{-1} (*i.e.* 100% was equivalent to 7.94 mgO_2 L^{-1} for a 28°C temperature and 0 salinity).

Experimental procedure –The fish were starved the morning before being transferred individually (late afternoon) to one of the two swimming respirometers for 24hrs before the swimming challenge. Each experimental trial consisted of challenging two fish in parallel. Each individual fish was left undisturbed with a water flow of 0.25 BL s^{-1} for a night to permit recovery

from handling stress and acclimate to this new environment. The swimming challenge started by increasing water flow by steps of 1.5 BL s^{-1} from 0.5 to 12.5 BL s^{-1}. Each step lasted 15 min, during which fish MO_2 was measured. Note that between 2 steps, O_2 is renewed; and that each time, it takes 3 minutes to progressively increase the water flow to reach the next step. The experiment stopped when the fish fatigued, i.e. when it did not manage to swim against the current and stay on the honeycomb. Speed was then decreased to 0.25 BL s^{-1} for a recovery period of 2 h. Fish were then removed from the swimming respirometer and anaesthetized using tricaine. Zebrafish are placed into a beaker containing 0.168 mg/mL of tricaine (3-amino benzoic acidethylester, Sigma-Aldrich, A5040, stock solution at 4 mg/mL dissolved in distiller water and stored at -20°C) freshly dissolved in system water. Fish progressively stop moving and we consider that they are anesthetized when they stop reacting to an external stimulation (e.g. gently taping on the bench close to the beaker). Standard and total length, mass and sex of each individual were determined; characteristics of the fish tested in the swim tunnel are described in Table S3. Before and after each trial, a blank measurement was performed to quantify microbial oxygen consumption in the swimming respirometer. The average of these two values was subtracted from the measured oxygen consumption. After each individual test, equipment was fully cleaned to reduce microorganism development. Each fish was tested once. Note that during swimming challenge experiment, fish are maintained in the same water conditions (temperature, pH, osmolarity…) than in their original animal facility.

Critical swimming speed - The critical swimming speed U_{crit} was calculated according to the formula of Brett (1964):

$U_{crit} = U_t + t_1 * t^{-1} * U_1$

where U_t (in BL s^{-1}) is the highest velocity maintained for an entire step, t_1 (in min) is the time spent until the exhaustion of fish at the last step, t (in min) is the swimming period for each step (i.e. 15 min in the present study) and U_1 is the increment velocity (1.5 BL s^{-1}).

Oxygen consumption (MO_2) measurements - Oxygen consumption MO_2 is expressed in mg O_2 g^{-1} h^{-1} and calculated using the following formula:

$MO_{2meas} = \Delta [O_2]. V. \Delta t^{-1} . M_{meas}^{-1}$

where Δ[O2] (in mg O_2 L^{-1}) is the variation in oxygen concentration during the measurement period Δt (in h), V (in L) is the volume of the respirometer minus the volume of the fish and M_{meas} (in g) is the fish mass measured. An allometric relationship exists between oxygen consumption and body mass, which permits correction of MO_{2meas} using the following formula:

$MO_{2cor} = MO_{2meas.} (MO_{2meas}. M_{cor}^{-1})^{1-b}$

where MO_{2cor} (in mg O_2 g^{-1} h^{-1}) is the oxygen consumption related to a standard fish of 0.1 g (M_{cor}), MO_{2meas} (in mg O_2 g^{-1} h^{-1}) is the oxygen consumption estimated for experimental fish whose mass was M_{meas} (in g) and b is the allometric scaling exponent describing the

relationship between oxygen consumption and body mass was calculated according to Lucas et al. (2014).

References

Brett, J.R. (1964). The respiratory metabolism and swimming performance of young sockeye salmon. J. Fish. Board Canada *21*, 1183–1226.

Charvet, B., Guiraud, A., Malbouyres, M., Zwolanek, D., Guillon, E., Bretaud, S., Monnot, C., Schulze, J., Bader, H.L., Allard, B., et al. (2013). Knockdown of col22a1 gene in zebrafish induces a muscular dystrophy by disruption of the myotendinous junction. Development *140*, 4602–4613.

Fry, F. E. J. (1971). The effect of environmental factors on the physiology of fish. In Fish Physiology, Vol. VI (Hoar, W. S. & Randall, D. J., eds), pp. 1–98. New York, NY: Academic Press.

Hammer, C. (1995). Fatigue and exercise tests with fish. Comp. Biochem. Physiol. Part A Physiol. 112, 1–20.

Lucas, J., Schouman, A., Lyphout, L., Cousin, X., and Lefrancois, C. (2014). Allometric relationship between body mass and aerobic metabolism in zebrafish Danio rerio. J. Fish Biol. *84*, 1171–1178.

Lucas, J., Percelay, I., Larcher, T., and Lefrançois, C. (2016). Effects of pyrolytic and petrogenic polycyclic aromatic hydrocarbons on swimming and metabolic performance of zebrafish contaminated by ingestion. Ecotoxicol. Environ. Saf. *132*, 145–152.

Supplementary Figures

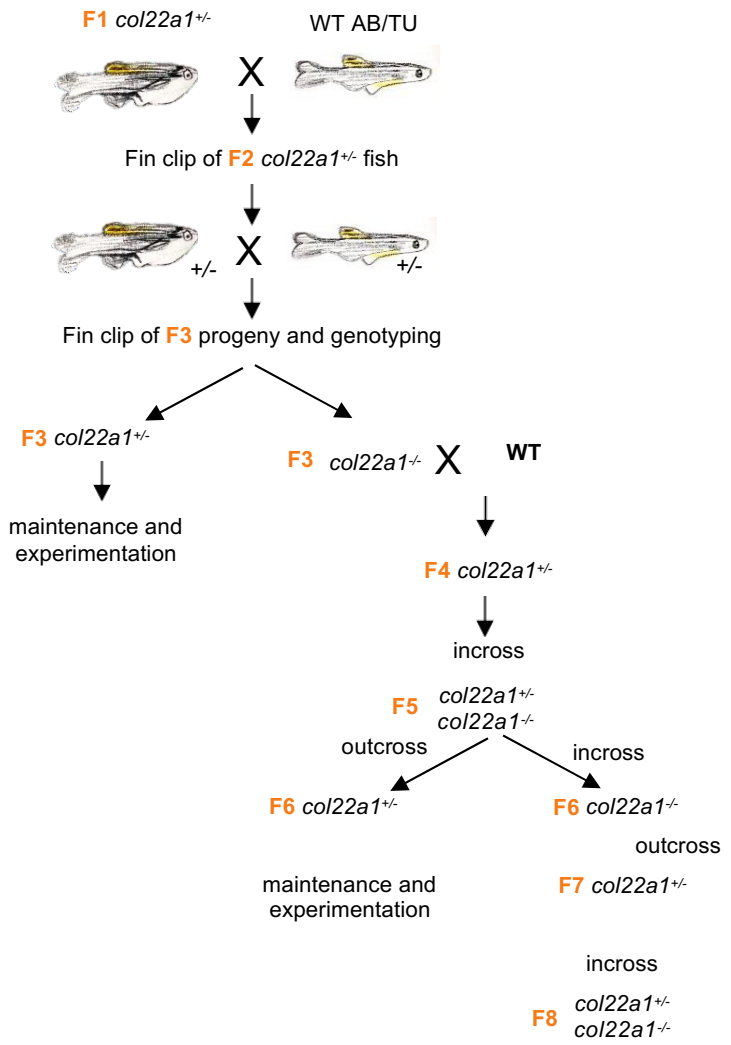

Figure S1: CRISPR-Cas9 *col22a1* lines - generation, crossing and maintenance. The same protocol has been applied to the two mutant lines (*col22a1*^{vWA} and *col22a1*^{TSPN}).

Supplementary Tables

Table S1: List of primers. For col22a1, the domains in which the primer sequences have been designed are indicated into brackets: COL5, collagenous domain 5; TSPN, Thrombospondin-1 N terminal-like domain; vWA, von Willebrand-like domain.

Gene	Primers
col1a1	*F-5'CTGCAAGAACAGCATTGCAT3'* *R-5'TAGGCAGACGGGATGTTTTC3'*
col12a1a	*F-5'AGGGCTCGTCTGTGTCTGAT3'* *R-5'GTTTTGCAGGATGACCGAGT3'*
col12a1b	*F-5'CTCCTCAGGACAAGGAGCAC3'* *R-5'GCACCAGCTTTTCTCCAGAC3'*
col14a1a	*F-5'TGCTCATTTCTGAGGTGACG3'* *R-5'GCGAACACTGCAATCTCGTA3'*
col14a1b	*F-5'GACCACGCTTCCTCTGACTC3'* *R-5'AGGTTACGCAGCTCCACTGT3'*
col21a1	*F-5'CTGGACCTGAGGGACGAC3'* *R-5'CCGATCGGAGGATGTCTCT3'*
*col22a1(*vWA*)*	*F-5'CAAGTGTGGGCAAGGAGAAT3'* *R-5'CGTTTGACCTCCTCCAATGT3'*
*col22a1 (*COL5*)*	*F-5'AGATGGAGCGGACGGTTT 3'* *R-5'CTGGTGGGCCTTCATCTC3'*
col22a1 (TSPN*)*	*F-5'CATCCAGGGGAAAACTGTCA3'* *R-5'CCATCCTCTGCAGGTCAAAG3'*
dag1	*F-5'TGTTGGAGCCTCTGTTACCC3'* *R-5'TGGGTTTCTTTGGAGGTCTCT3'*
fn1b	*F-5'ATTCAACGCACGTTCCTACC3'* *R-5'TAATTTTGCCCTTGCCTGAC3'*
itga7	*F-5'CAGCTGGTACCCAAACACG3'* *R-5'CACAGAGTACCCGAATGAGGA3'*
lama2	*F-5'CCACTGGGGTCACGACAT3'* *R-5'CGGTGTTCAGGTTACACTGC3'*
lama4	*F-5'AATCACGTTGTGGGGTCTGT3'* *R-5'ACCGATAAACACTGGCGAAC 3'*
polr2d	*F-5'CCAGATTCAGCCGCTTCAAG3'* *R-5'CAAACTGGGAATGAGGGCTT3'*
scxa	*F-5'*ATTCGAGAGCCTTGTGGAGA*3'* *R-5' CCCCCTACACTGGATTTCCT3'*
scxb	*F-5'*AGCGAGAACGAACGAACAGT*3'* *R-5'* TGGTGGTGATGAAACAAGGA*3'*
thbs4b	*F-5'GAGGAGGAAGACTGGGAGTGT3'* *R-5'GTCCTCTGGGATGGTGTCAT3'*
tnmd	*F-5'*ACCGTTACTGTCGGCGATAC*3'* *F-5'*GTCTATGCAAACCCCTGAGC*3'*

Table S2: List of primary (in bold) and secondary antibodies used in this study.

Primary and Secondary antibodies	Reference	Dilution used
anti-ColXXII	polyclonal, rabbit (home-made[1])	1:1000
anti-ColXII	polyclonal, guinea pig (home-made[2])	1:250
F310, myosin light chain 1	DSHB, F310, monoclonal, mouse	1:20
anti-rabbit Alexa Fluor 488	Invitrogen, A11034	1:500
anti-mouse Alexa Fluor 488	Invitrogen, A11029	1:500
anti-guinea pig Alexa Fluor 488	Invitrogen, A11073	1:500
anti-rabbit Alexa Fluor 546	Invitrogen, A11035	1:500

[1]Charvet B, Guiraud A, Malbouyres M, Zwolanek D, Guillon E, Bretaud S, Monnot C, Schulze J, Bader HL, Allard B, Koch M, Ruggiero F. 2013 Knockdown of col22a1 gene in zebrafish induces a muscular dystrophy by disruption of the myotendinous junction. Development, 140:4602-13.
[2]Bader HL, Charvet B, Veit G, Driever W, Koch M and Ruggiero F. 2009 Zebrafish collagen XII is present in embryonic connective tissue sheaths (fascia) and basement membranes. Matrix Biol 28:32-43 *doi*: 10.1016/j.matbio.2008.09.580

Table S3: Biometry of fish used for swimming tunnel step protocol. M, male; F, female; SL, standard length; TL, total length.

Fish genotype and number	Sex	Weight (g)	Morphometry			
			SL (cm)	TL (cm)	Thickness (cm)	Height (cm)
WT1	M	0.468	3.1	3.9	0.5	0.7
WT2	M	0.459	3.2	3.9	0.5	0.7
WT3	F	0.433	3.1	3.8	0.4	0.7
WT4	F	0.376	2.7	3.3	0.3	0.7
WT5	F	0.426	3.3	4	0.5	0.7
WT6	F	0.453	3	3.7	0.4	0.7
WT7	F	0.446	3	3.6	0.3	0.7
WT8	F	0.578	3.2	3.9	0.4	0.8
WT9	M	0.427	3.1	3.8	0.3	0.6
WT10	M	0.677	3.2	4.1	0.5	0.7
col22a1$^{TSPN-/-}$ 1	M	0.462	3	4	0.5	0.7
col22a1$^{TSPN-/-}$ 2	M	0.420	3.3	3.8	0.5	0.7
col22a1$^{TSPN-/-}$ 3	F	0.369	3.1	4.2	0.5	0.7
col22a1$^{TSPN-/-}$ 4	F	0.437	3	3.7	0.5	0.7
col22a1$^{TSPN-/-}$ 5	M	0.369	3	3.5	0.4	0.7
col22a1$^{TSPN-/-}$ 6	M	0.370	2.8	3.8	0.4	0.7
col22a1$^{TSPN-/-}$ 7	F	0.769	2.5	3.3	0.5	0.7
col22a1$^{TSPN-/-}$ 8	F	0.398	3	4	0.4	0.7
col22a1$^{TSPN-/-}$ 9	F	0.331	3.1	3.5	0.4	0.7
col22a1$^{TSPN-/-}$ 10	F	0.584	3.1	4	0.6	0.8
col22a1$^{TSPN-/-}$ 11	M	0.389	2.8	3.5	0.4	0.6
col22a1$^{TSPN-/-}$ 12	F	0.604	3.4	3.7	0.4	0.7
col22a1$^{TSPN-/-}$ 13	M	0.422	3	3.5	0.4	0.7

Supplementary Movies

Movie 1: Swimming capacity of a 2wpf WT larva (*col22a1*$^{TSPN+/+}$). The swimming capacity and postural behavior were recorded at different time intervals using a Zeiss Axiozoom V16 stereoscopic microscope with a digital camera system.

Movie 2: Swimming capacity of 2wpf of a class 1 mutant larva (*col22a1*$^{TSPN-/-}$). The swimming capacity and postural behavior were recorded at different time intervals using Zeiss Axiozoom V16 stereoscopic microscope with a digital camera system.

Movie 3: Swimming capacity of 2wpf of a class 2 mutant larva (*col22a1*$^{TSPN-/-}$). The swimming capacity and postural behavior were recorded at different time intervals using a Zeiss Axiozoom V16 stereoscopic microscope with a digital camera system.

Movie 4: Swimming performance of a 6mpf wildtype sibling (col22a1$^{TSPN+/+}$) fish using a high-speed camera MiroM310. The video was acquired during swimming step protocol experiment at 5BL.s^{-1} water flow and slowed down 10 times vs real speed.

Movie 5: Swimming performance of a 6mpf class 1 mutant fish (col22a1$^{TSPN-/-}$) using a high-speed camera MiroM310. The video was acquired during swimming step protocol experiment at 5 BL.s-1 water flow and slowed down 10 times *vs* real speed.

Movie 6: Swimming performance of a 6mpf wildtype sibling (col22a1$^{TSPN+/+}$) fish using a high-speed camera MiroM310. The video was acquired during swimming step protocol experiment at 8BL.s^{-1} water flow and slowed down 10 times vs real speed.

Movie 7: Swimming performance of a 6mpf class 1 fish (col22a1$^{TSPN-/-)}$ using a high-speed camera MiroM310. The video was acquired during swimming step protocol experiment at 8 BL.s-1 water flow and slowed down 10 times vs real spee